An Investigation of Early Radiation Damage in Exposed Eye-Lenses of Rainbow Trout

by

Marta Kocemba

A thesis submitted to the
School of Graduate and Postdoctoral Studies in partial
fulfillment of the requirements for the degree of

Master of Applied Science

in

Nuclear Engineering

Faculty of Energy Systems and Nuclear Science
University of Ontario Institute of Technology

Oshawa, Ontario, Canada

August 2019

THESIS EXAMINATION INFORMATION

Submitted by: **Marta Kocemba**

Master of Applied Science in **Nuclear Engineering**

An Investigation of Early Radiation Damage in Exposed Eye-Lenses of Rainbow Trout

An oral defence of this thesis took place on August 7, 2019 in front of the following examining committee:

Examining Committee:

Chair of Examining Committee:	Dr. Kirk Atkinson
Research Supervisor	Dr. Anthony Waker
Examining Committee Member	Dr. Edward Waller
Examining Committee Member	Dr. Brian Ikeda
Thesis Examiner	Dr. Denina Simmons, Faculty of Science

The above committee determined that the thesis is acceptable in form and content and that a satisfactory knowledge of the field covered by the thesis was demonstrated by the candidate during an oral examination. A signed copy of the Certificate of Approval is available from the School of Graduate and Postdoctoral Studies.

Abstract

The objective of this work is to contribute to the study of radiation effects in non-human biota and potentially to the study of eye-lens damage in humans by investigating the effects of low-energy X-rays on the lenses of rainbow trout. Lenses were cultured and irradiated to doses up to 2.210 Gy with low-energy X-rays of 40 kV. Laser focal analysis was used to track changes in focal lengths across the lenses post-irradiation. The purpose of this study was to determine whether focal length variability (FLV) could give an indication of the early effects of radiation on lens health. Five dose points between 0.044 Gy to 2.210 Gy were observed. None of the groups showed differences in focal length variability compared to the control group (FLV of 0.14 mm $\pm$ 0.03 mm for the 2.210 Gy group compared to 0.13 mm $\pm$ 0.02 mm for the control group).

Keywords: rainbow trout; X-ray radiation; lens focal analysis

Declaration of Authorship

- I hereby declare that this thesis consists of original work of which I have authored. This is a true copy of the thesis, including any required final revisions, as accepted by my examiners.
- I authorize the University of Ontario Institute of Technology to lend this thesis to other institutions or individuals for the purpose of scholarly research. I further authorize University of Ontario Institute of Technology to reproduce this thesis by photocopying or by other means, in total or in part, at the request of other institutions or individuals for the purpose of scholarly research. I understand that my thesis will be made electronically available to the public.

Signed: 

Date: August 15 2019

Statement of Contributions

I hereby certify that I am the sole author of this thesis and that no part of this thesis has been published or submitted for publication. I have used standard referencing practices to acknowledge ideas, research techniques, or other materials that belong to others. Furthermore, I hereby certify that I am the sole source of the creative works and/or inventive knowledge described in this thesis.

Acknowledgements

First and foremost, I would like to extend my deepest appreciation and gratitude to Dr. Anthony Waker, whose endless enthusiasm for research and exemplary attitude as an advisor are everything I hope to achieve as a scientist and a scholar.

Thank you to my friends and family who have always been encouraging and supportive of my endeavours. Thanks also to the turtles and frogs of the campus pond, for providing the endless hours of distraction and procrastination that are necessary when writing a thesis.

The research performed in this thesis has been funded by the Natural Sciences and Engineering Research Council of Canada (NSERC) and the University Network of Excellence in Nuclear Engineering (UNENE).

Contents

List of Figures

List of Tables

Chapter 1

Introduction & Background

1.1 Motivation for the Study of Fish Eye-Lenses

The research topic addressed in this work has been motivated by the recent interests of the International Commission on Radiological Protection (ICRP) in the areas of eye lens dosimetry as well as environmental protection. ICRP has released recommendations for lowering the dose limits for eye lenses in occupationally exposed workers based on a review of recently available epidemiological data. ICRP has also emphasized the importance of assessing the current degree to which the environment and non-human biota are being protected from ionizing radiation. These topics and their intersection will be explained in the following sections.

1.1.1 Interest in Implementing New Lens Dose Limits

The potential effects of radiation on the lens of the eye have been under consideration by ICRP since 1950, when there was a potential relationship identified between radiation dose and cataract formation [1]. In 1955, ICRP provided its first recommendation for a dose limit to the lens of the eye, and these recommendations were updated over the next several decades, as more research became available [2]. The most recent change occurred in 2011, when ICRP's *Statement on Tissue Reactions* proposed a new 0.5 Gy threshold for tissue effects in the eye lens, as well as a new

recommendation for occupational exposure of 20 mSv/a to the eye lens averaged over five years, with no single year exceeding 50 mSv [3] [4].

Since this time, regulatory bodies have been assessing the possibility of implementing new dose limits to the lens of the eye based on these recommendations. In 2013, the Canadian Nuclear Safety Commission (CNSC) indicated its intention to lower the annual limit to the eye lens in occupationally exposed workers from 150 mSv/a to 20 mSv, in agreement with ICRP's recommendation. The new regulatory limits have not yet been implemented; stakeholders are in the process of assessing what changes need to be made to support new dose limits [5].

This change has stimulated renewed interest in eye-lens dosimetry and has led to a significant amount of scientific work concerning the effects of radiation on the eye-lens. These studies can then inform the regulatory bodies in further decision making.

1.1.2 Interest in the Radioprotection of the Environment

ICRP has also been addressing the issue of environmental radiation protection over the course of several publications. ICRP's stance on protecting the environment from radiation was stated in 1991, and was based on the assumption the environment is sufficiently protected from radiation as long as adequate radiation protection measures are taken to protect humans [6]. However, ICRP created a Task Group whose goal it was to review the necessity of protecting the environment directly. The report produced from this review was released in 2003 as ICRP Publication 91, and states that it is indeed necessary to provide a system for radiological assessment and protection of non-human biota in the environment. The goals of such a system are to minimize radiation effects that could cause early mortality, and to conserve biodiversity and the ecological health of natural habitats [7].

The current environmental protection system is described by ICRP Publication 108 [8]. The basis of this system is the concept of Reference Animals and Plants, which is consistent with the system used for human radiation protection (i.e., Reference Man). A Reference Animal or Plant is defined for several major taxonomical groups

based on the current availability of data and the probability of amassing more data in the future, as well as on geographical representation. In other words, Reference Animals and Plants were chosen based on how common they are in different types of ecosystems, and how popular they already are in biological studies (which can be used to predict whether more data will be available in the future).

1.1.3 Eye Lens Health in Non-Human Biota

The two motivating topics in this work are the recent interests in radiation effects on the eye-lens, and in the effects of radiation on non-human biota, as described above. The intersection of these topics is the effect of radiation on the eye-lens of non-human biota.

One of the goals of ICRP's environmental protection system is to minimize radiation effects that could cause early mortality in non-human biota. The obvious implication of this objective is that radiation exposures that would result in lethal doses to individuals of a particular species need to be avoided, since this would be mortality directly caused by radiation dose. However, there are also situations in which radiation effects could indirectly cause early death in an individual. One of these situations considers the possibility of radiation leading to full or partial blindness.

Many species depend heavily on their vision for feeding, so damage to the lens could lead to an individual's inability to feed. Additionally, good eyesight would give animals a better chance to notice and avoid natural predators. Both these factors contribute to the well-being of the animal, and ultimately its ability to survive. If an animal were to develop sight-impairing cataracts that hindered successful feeding and predator evasion, then it is possible that the animal could die from the consequences of these effects (i.e., from starvation or from being eaten by a predator that it would have been able to avoid under normal circumstances). Even though radiation dose would not be the cause of death in the usual sense, the death would still be attributable to a radiation effect. This type of indirect mortality from radiation should also be considered in an environmental radiation

protection assessment.

Radiation effects in non-human biota would likely be due to the release of radioactive material into the environment. This situation could occur as a result of an accident at a nuclear reactor site, since nuclear reactors are generally situated at the shore of a body of water. Potential radioactive contaminants could then disperse through the aquatic environment, and the animals living in that body of water would receive radiation dose through both external and internal exposure. Studying radiation effects in aquatic biota (such as fish) could be helpful in contributing to the body of knowledge available for decision-making in the area of environmental radioprotection.

Studying radiation effects in fish eye lenses could also be useful towards general eye lens dosimetry knowledge. Generally, vertebrates have the same eye structure and physiology since this version of the eye evolved before the separation of vertebrates from other phyla. Therefore, the eyes of vertebrate fish are functionally and anatomically similar to human eyes [9]. This leads to the possibility of having general discussions about vertebrate eyes and lenses, with the implication that conclusions drawn from one type of vertebrate eye could be applicable to other types of vertebrate eyes [10]. In this way, knowledge gained from studying fish eye lenses could be transferable towards knowledge of human eye lens function.

Therefore, apart from the potential of contributing to the understanding of effects in the human eye, research on radiation effects on the eye-lens of fish has obvious relevance for aquatic species in heavily contaminated bodies of water, such as would likely occur following a severe reactor accident. This work could be helpful in contributing to the current knowledge in both eye lens dosimetry and environmental radioprotection.

1.2 Background to Vertebrate Eye Lens Research

1.2.1 Anatomy of Vertebrate Eyes

Vertebrate eyes share the same general anatomy: the eyeball (sclera) has a cornea at the front to let light in, a lens to focus the light, and a retina onto which light falls to form an image (Figure 1.1). The space inside the sclera is filled with a clear gel called the vitreous body. In terrestrial vertebrates, the cornea provides some refraction of light, since there is a difference in refractive power between the air and the cornea. This refracted light is then further refracted by the lens.

However, the refractive index (RI) of the cornea is very similar to that of water ($RI_{cornea} = 1.38$ vs. $RI_{water} = 1.33$), so the cornea provides no useful refraction in the optical systems of aquatic vertebrates [10] [11]. To make up for the relative loss in refractive power, fish eye lenses provide stronger refraction. To provide a stronger refraction, the curvature of the lens in stronger in fish, resulting in a spherical lens. This is one of the main differences in optical function between aquatic and terrestrial vertebrates [12]. Because the lens is virtually entirely responsible for refracting light to form images, any damage to the lens would have a direct impact on the visual capacity of the fish. Additionally, the lens is considered to be particularly susceptible to damage from its environment because the lens generally sits immediately behind the cornea, instead of behind a pupil like in terrestrial vertebrates [11] [13].

The lens is held in place by several muscles and ligaments. The most prominent are the retractor lentis muscle and the central suspensory ligament, which are supported by a set of four thinner ligaments [11].

1.2.2 Culturing Eye Lenses for *in vitro* Organ Culture

The eye-lens itself is a living organ and consists of a surface of epithelial cells, which undergo mitosis throughout the entire lifetime of the animal. The epithelial cells differentiate into lens fibre cells and migrate from the surface of the lens towards

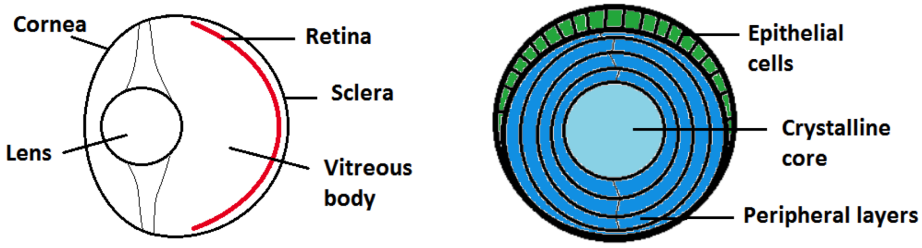

FIGURE 1.1: A simplified diagram of a vertebrate eye (left) and vertebrate lens (right) showing the basic anatomy.

the centre, elongating and layering over one another. As epithelial cells differentiate into fibre cells, they lose their organelles and nucleus. Fibre cells move towards the core of the lens, at which point they are no longer living cells that contribute to metabolic processes in the lens [14] [15] [16]. The basic lens cellular structure is shown in Figure 1.1.

Biological *in vitro* experiments are generally performed as a type of tissue culture. This can be in the form of cell culture (where the histological structure of a tissue is not maintained) or organ culture (where the tissue structure is maintained). Both these types of culture have advantages and disadvantages, but perhaps the most obvious advantage to organ culture is that a particular tissue can be cultured and studied in the same form that it exists *in vivo*. This is different from cell culture, where cell types are cultured and studied separately (or combined with other cell types in an attempt to allow the cell types to interact with one another, mimicking *in vivo* settings to an extent) [17].

Organ culture is difficult to perform correctly because of the many considerations and constraints that are not present in cell culture. Generally, the most difficult aspect of organ culture is the lack of a vascular system. *in vivo*, tissues are usually supplied with oxygen and nutrients via the blood supply and its structure of blood vessels. However, in organ culture, this process is generally limited to diffusion [17].

In eye-lenses, this does not present a problem for culturing. The lens is not vascular, and its metabolic processes occur mainly in the outer layer of epithelial cells and

only the newly-differentiated fibre cells [10]. Therefore, *in vivo*, the lens does not need to be supplied with nutrients other than what is diffused from the vitreous body into the outer layers of the epithelial and fibre cells. This is consistent with the knowledge that the core of the lens is actually non-living, and thus has no need to have access to nutrients and oxygen for metabolic processes.

Organ culture of eye lenses can be performed in a way that allows for the assessment of optical quality. Details of these methods will be discussed in Chapter 2. Therefore, the basis of this work will be culturing the lenses of fish eyes in order to assess radiation effects in the eye-lens from the perspective of environmental radioprotection.

Chapter 2

Literature Review & Statement of Work

The literature that has been consulted in the development of concepts and procedures for this work and for its analysis can generally be divided into two topics.

1. A review of the literature concerning the assessment of damage to eye-lenses, which provides the basis for the design of measurement and analysis procedures. This information was used to hypothesize about the type of damage that would be likely to occur to a lens in the early stages of reaction to a stressor. It also provides information about the types of analysis used to measure this damage. This includes the assessment of lens damage in general, and not exclusively radiation-specific damage.
2. A review of the current knowledge of radiation effects to the eye-lens, which addresses the substantial difference between lens studies and lens cell studies (i.e. organ culture vs. cell culture). This includes the relationship of human studies and non-human studies, which highlights the importance of non-human eye-lens research, and demonstrates the gap that can be addressed by the work described in this thesis.

These topics will be explained in detail in the following sections and concluded with the statement of work for the set of experiments presented in this thesis.

2.1 Methods of Damage Assessment in Eye Lens Toxicology

Eye lens toxicology is a field of study that aims to measure damage to the lens of the eye. There are several types of damage assessment methods in eye lens toxicology that can be classified into either intact eye lens assessment or cellular assessment. Specific methods within these categories will be described in the following sections.

2.1.1 Intact Eye-Lens Assessment

There are relatively few methods of assessing lens damage in vivo (i.e., while the animal is still alive). A common method that has been used for several decades is slit-lamp biomicroscopy, which allows the lens to be observed by shining a thin beam of light into the eye [18]. Photorefractometry has also been used for in vivo evaluation of relative refraction across the lens, and creates a visualization of lens refraction by detecting the reflection of light that has been sent into the eye [19] [20]. However, these methods are not useful for in vitro measurements, since they rely on having the light that reflects from the back of the eye after having passed through the lens. Therefore, lens measurement methods specifically developed for excised lenses will be considered.

Intact eye lenses can be assessed immediately after excision from the eye, or they can be put into organ culture for more long-term assessment. Organ culture requires a carefully designed dissection procedure in order to maintain sterile conditions and avoid damage to the lens. Once lenses are excised, they need to be kept in a specific solution of nutrients that will allow their usual metabolism to continue, thereby keeping the lenses alive. This appears to be unnecessary in the very short term, based on studies where lens measurements have successfully been made after excision without the need for culture medium [21] [22]. However, using these methods involves applying the stressor (which causes the lens damage) to the animal in vivo before euthanization.

Studies assessing in vitro damage to the intact eye-lens exist for both mammalian and aquatic vertebrates, which require different culturing procedures because of different physiologies. Organ culture of mammalian eye lenses (or any culturing technique for any mammalian tissue) requires an incubator to keep the tissue at a biologically appropriate temperature [17]. However, since many vertebrate fish live in cool water, incubation is unnecessary, and in fact, the culturing is done at cooled temperatures for a wide variety of species including rainbow trout [23].

The focal analysis of intact eye-lenses consists of measuring the refraction across a lens and is a very common method in lens assessment. The earliest versions were done by simply observing a grid through the lens, which progressed to the use of thin laser light beams to track refraction changes across the lens diameter [24]. This method was then improved upon and automated, adding the capacity to assess beam spread [25] [26]. This system also included the assessment of transmittance to show changes in refraction. While lowered transmittance of a beam of light through the lens could indicate the early stages of clouding, an increase in transmittance would suggest changes in refraction occurring on a scale smaller than the beam diameter. Measuring an increase in light intensity in some pixels of the digitizer means that the refraction of some parts of the beam has changed, thus causing an 'overlap' of light, which manifests as more pixel stimulation. However, while the automated system certainly provides some advantages in damage analysis, the method is essentially the same as the earlier, manual versions of observing the refraction of individual laser beams.

The use of fluorescence assays with intact lenses has also become popular as a method of assessing lens condition, often together with laser analysis of refraction. A particular dye sold commercially as Alamar Blue has been used across several lens damage studies to assess the viability of the epithelial cells on the surface of the lens. Alamar Blue is non-fluorescent, but is metabolized by functioning cells to a fluorescent compound. Therefore, by measuring the fluorescence of a particular sample treated with Alamar Blue, a quantifiable measure of cellular activity can be measured [27]. This method has been used to assess lens health as well as lens damage from ultraviolet (UV) radiation, surfactants, and other irritants [28] [29].

2.1.2 Cellular Assessment

Cellular assessment is generally performed at the end-point of a study that uses intact lenses since the lenses must be sacrificed for lens cells to be obtained. In general, the purpose of cellular assessment is to monitor the function and viability of lens cells outside of the context of overall lens health. This can be done by measuring the metabolic activity of the cells.

Cellular metabolic activity can be measured in several ways, many of which have been used in eye lens studies. Some studies have simply measured the ratios of certain cations present in lens cells that have been incubated at different conditions based on the understanding that certain metabolic processes change the concentrations of specific ions in the cell [30]. This method can be extended by measuring specific compounds such as lactic acid production or glutathione, which both represent the activity of certain metabolic processes in the lens [31].

Specific enzyme analysis has been used when a particular damage pathway has been identified. For example, the effects of UV-A radiation on the eye-lens have been reported in terms of the loss of activity of particular enzymes, and this allowed for the design of experiments that quantify this effect [32] [33]. Another example of a specific and relevant cellular assay for specific radiation damage is the immunofluorescence assay that allows γH2AX (a marker of DNA double-strand breaks) to fluoresce and, therefore, be quantified [34] [35].

Microscopy has also been useful in assessing changes to lens cells, though this is a qualitative assay and has limited applications. In some applications, the lens sutures (i.e., the junctions where multiple lens cells meet) have been assessed for changes following microwave irradiation, since these are the sites responsible for cataracts caused by what were thought to be related pathways [36].

Cellular assays in lenses are often specific and assess target cell functions as opposed to general lens health. Many of these assays also require laboratory equipment that is more specialized than what is required to perform many of the intact-lens assessments, as described in the previous section. Though these assays are very useful for analyses of specific metabolic or cellular processes, they are targeted,

which means that the particular damage pathway must be known ahead of time in order to design the assessment. This can often pose a limitation for the type of cell response that can be studied.

2.1.3 Summary

A laser scanning apparatus was chosen instead of cellular assessment as a damage measurement method for the work in this thesis. While it is straightforward to build and use a simple laser scanning device as previously described, this is not the case with specialized enzyme assay techniques. Also, using cellular assay techniques requires sacrificing the lens, whereas laser scanning is non-destructive, and the same lens can be measured several times. Therefore, the usefulness of laser scanning will be explored and its limitations will be established before moving to more specialized and work-intensive techniques.

2.2 Radiation Effects on Eye-Lenses

The following sections will provide a summary of the work that has been done thus far in understanding radiation effects in eye-lenses. The relationship between human and non-human eye lens work will also be discussed.

2.2.1 Human vs. Non-Human Eye-Lens Work

As described in Section 1.1.1, there has been significant interest in studying the radiosensitivity of the eye-lens. Radiosensitivity of tissues has been attributed in large part to mitotic activity, with the understanding that tissues made of actively dividing cells are sensitive to radiation effects, mostly in the form of cell killing [34][37]. However, there has been some discussion about whether cell killing is actually the mechanism that causes lens damage [38].

Data on radiation effects in human eye-lenses is somewhat scarce, since there is a relatively small number of groups that can be studied. Human lens data is taken from epidemiological studies of relevant populations. Some of the data on eye lens dose and cataract formation are related to cancer patients who develop cataracts as a result of receiving radiation treatment where the eyes cannot be shielded [39]. Much of the data is from epidemiological work based on atomic bomb data and Chernobyl data, where the incidence of cataract formation has been related to the best estimates of dose received by various individuals. Other occupationally exposed populations included in epidemiological studies include pilots, astronauts, and radiation technologists. Non-occupationally exposed groups include populations living in buildings built with Co-60 contaminated steel in Taiwan. The data from these groups was important in ICRP's decision to recommend lower eye-lens dose limits) [4]. Since then, more data has become available based on Mayak workers (a cohort of 22,377 workers followed for several decades) and agreed with ICRP's decision, and suggested a relative risk at even lower lens doses (0.28 Gy) [40].

Overall, human eye lens studies are generally based on cataract incidence and, therefore, do not offer much insight into assessing early radiation damage to eye lenses. However, as described in Chapter 1, most vertebrates share the same ocular anatomy and physiology. Therefore, in vivo and in vitro lens studies in non-human vertebrates can also contribute significantly to understanding radiation effects in human eye-lenses.

Animal studies that have contributed to eye lens knowledge in humans have been based on rabbit, rat, and mice studies [41] [42]. Most of this work is focused on cataract formation, since cataracts are the major interest in human lens work.

A significant number of non-human eye-lens studies are based specifically on the early response of the lens to radiation, and do not assess cataracts within their scope. Bovine and porcine lenses are often used in these studies. Vertebrate fish are also useful for these studies, since their ocular system depends very heavily on the refractive capability of the lens.

Overall, studies on human eye-lenses are limited to epidemiological work due to the

nature of in vitro studies, but non-human vertebrate eye-lenses are often used in their stead. This is based on the anatomical similarities between the ocular systems of most vertebrates. Since studies on non-human eye-lenses can be very useful for contributing to the knowledge of radiation effects in human lenses, the sections describing radiation effects in eye-lenses will include human as well as non-human research.

2.2.2 Radiation Effects on Intact Eye Lenses

Radiation effects in intact eye lenses have been studied in many species, both mammalian and aquatic. However, most of the radiation effects documented for intact lenses, as presented here, have been focused on ultraviolet radiation, with some exploration into microwave radiation. In general, there is a lack of research assessing the effects of ionizing radiation (other than ultraviolet) on intact eye-lenses. Studies involving vertebrates in general will be discussed, since knowledge about vertebrate eye-lenses is transferable to some degree to the understanding of human eye-lenses.

Radiation studies on eye-lenses in mammals have been mostly focused on UV radiation in both the UV-A and UV-B spectra. In bovine lenses, UV radiation studies were the preliminary work that showed the efficacy of using a laser system to evaluate lenses based on their refractive capacity [43] [44]. These studies have shown that there is a measurable change in refraction across the lens after a lens is irradiated with UV radiation. Importantly, this damage was measurable before the onset of any visible opacities. Also, changes in refraction could be tracked over several days during which time the lenses were shown to recover from the initial damage and regain their refractive capacity. It was demonstrated that these changes could be expressed qualitatively and quantitatively.

UV radiation effects have also been measured in porcine lenses. Lenses were irradiated with UV radiation and their focal lengths were evaluated by laser scanning over the course of four weeks post-irradiation [36]. The laser system was successful in showing quantitative changes in optical quality over the course of the study.

The effects of microwave radiation have also been assessed in bovine lenses using the laser scanning system to measure changes in refraction. Damage to lenses exposed to microwaves was successfully measured, and short-term recovery (within days of the radiation exposure) was also demonstrated [36].

UV radiation effects have also been studied extensively in teleosts. In many cases, teleost lens studies were specifically designed to gain understanding in the combined effects of UV radiation with other irritants and contaminants. This is generally from an environmental contamination perspective, where particular contaminants have not been shown to be harmful to lenses on their own, but do produce lenticular changes in the presence of UV radiation [29] [13]. This has obvious relevance in environmental toxicology studies. The lens damage in these studies has been successfully measured with the laser scanning system described previously, and the damage was shown to be measurable by tracking the focal lengths of many laser beams across the lens.

2.2.3 Radiation Effects on Lens Epithelial Cells

While cataract development studies have been ongoing for several decades, the response of lens cells to radiation is poorly understood [45]. As previously discussed, there is a significant difference between cell response to stress in cell culture compared to how those same cells react in vivo. Therefore, it can be difficult to relate lens cell culture work to macroscopic effects in intact lenses. Nonetheless, understanding the basic mechanisms is important since this will likely lead to understanding tissue effects as research progresses.

There has been a significant amount of work that has been done on human and animal lens epithelial cells (LECs) based on interest in the radiosensitivity of the lens. As previously described, the lens is considered to be radiosensitive because of its outer layer of epithelium that actively divides over the lifetime of the animal.

As previously discussed here, most of the radiation response work done with intact eye-lenses has been focused on UV radiation. UV radiation response has also

been studied in human LECs using several assay types, including clonogenic assay, Alamar Blue fluorescence, and immunofluorescent staining [46] [47].

However, LEC response to ionizing radiation has been studied for several vertebrate species, and this response has been measured in comparison with other cell types. In mice, it has been demonstrated that LECs have a higher radiosensitivity than others when compared to lymphocytes of the same species [48]. The radiosensitivity of human LECs has been compared to human lung fibroblasts, and this has shown that human LECs are actually less radiosensitive than lung fibroblasts [49]. The D-10 (the dose that leaves a cell population at 10% of its original number) for human LECs was shown to be 3.56 Gy, compared to 3.22 Gy for fibroblasts. This is an example of the type of research that had challenged ICRP's initial assumption that the lens was radiosensitive because of its susceptibility to cell killing. Irradiated LECs actually showed an increase in proliferation, and it is this effect that has been considered a possible cause for lens abnormalities [38]. Other human LEC studies have shown that a D-10 dose to these cells does not affect viability for colony formation, but does cause a delay in population growth [45]. This could have implications for a structure whose function relies on the successful implementation of a very specific pattern of cell arrangement.

Overall, much of the body of research that contributes to understanding radiation effects in eye lenses comes from lens epithelial cell studies. While it can be difficult to relate findings from cell studies to effects in the lens itself, the findings related to cell response to radiation can offer new avenues to consider in intact lens studies.

2.2.4 Summary

The work described in the literature shows that there has been a considerable amount of research effort put towards understanding the effects of ionizing radiation on lens epithelial cells. While this is helpful towards understanding the basic mechanisms through which radiation effects may occur, there can be significant difficulty in relating effects seen in cell culture to effects seen in the lens as a whole.

The present literature shows a good basis for the effects of ultraviolet radiation on

intact eye-lenses. However, there is a distinct lack of research on other ionizing radiation effects on intact eye-lenses. Therefore, new research that measures changes in refraction due to ionizing radiation other than ultraviolet would help increase the understanding of whole lens effects.

2.3 Objectives & Statement of Work

The purpose of this work is to determine whether there are early radiation effects in the eye-lens of rainbow trout (*Onchorhynchus mykiss*) that can be detected using a laser focal analysis system. 'Early' effects refers to damage preceding the formation of visible opacities or cloudiness, which is the more widely recognized form of lens damage, and generally occurs on a longer timescale than is being considered in this work.

The experiments will consist of excising lenses from the eyes of rainbow trout and culturing them so that they remain metabolically active. Lens health will be measured using laser focal analysis, which measures refraction across the diameter of a lens. The data from focal measurement can be expressed qualitatively through focal profile plotting, or quantitatively through the calculation of back vertex distance and focal length variability. The quantitative interpretation will be used to assess changes in the refraction of a lens after irradiation. This damage assessment method was chosen in part because a simple version of the apparatus is straightforward to build and implement, and also because the automated version of this method is widely used to measure changes in lens health from a variety of stressors.

The depth-dose profile, photon energy distribution changes, and beam spot sizes will be characterized for a low-energy X-ray generator (Amptek Mini-X). The Mini-X will then be used to irradiate lenses to several dose points up to 2 Gy. The lenses will be monitored daily for changes to their focal capacity until such a point that their physical condition is no longer suitable for laser analysis (i.e., when the time constraints of the culture method have been reached, and lenses have deteriorated). Statistical analysis of these results will be used to determine whether there are

measurable changes to the lenses' refractive capacity as a result of the irradiation.

To summarize, the objectives of this work are as follows:

- Develop a set of procedures that will allow lenses to be maintained in good health for long enough to perform short-term assessment. This includes a dissection procedure to excise the lenses without damaging them, a culturing procedure to maintain lens health and function, as well as sterilization procedures for both dissection and culturing.
- Characterize the Mini-X low-energy X-ray generator for dosimetry. This includes measuring the beam spot size, depth-dose profile, and photon energy distribution of the X-ray spectrum.
- Irradiate groups of eye-lenses to several dose points up to 2 Gy.
- Perform laser focal analysis on lens groups to determine whether there are any measurable changes in the refraction of irradiated lenses.

Chapter 3

Characterization Experiments

This chapter discusses all experimental procedures and methodologies used in this work. Some are based on methods used in literature (see Chapter 2), while some have been developed specifically for these experiments.

3.1 Dry Heat Sterilization Oven

Aseptic technique (i.e., performing work under sterile conditions) is important to in vitro culturing work. A main aspect of maintaining sterility is using sterile equipment, either by purchasing disposable, pre-sterilized plastic items or by sterilizing items in the laboratory. In these experiments, sterilization was performed using dry heat as described below.

Instruments and glassware were sterilized with dry heat using a Heratherm™ OGS60 Dry Heat oven from Thermo Scientific set to one hour at 180 °C [17] [50]. Dry heat sterilization, as opposed to the more common autoclaving (wet heat sterilization), is considered to be the best practice for sterilizing glassware and metal instruments [17] [51] .

Before being used for sterilizing laboratory equipment, the oven was verified for correct and consistent temperatures using an independent thermometer, whose readings were compared to the readings from the oven itself. The purpose of this verification was to confirm that the oven was reaching and maintaining the

temperatures required for sterilization of glassware and instruments that are used in aseptic procedures. The test also verified that the oven's internal temperature indicator was acceptably close to independently measured values. This was assessed by checking that the load in the middle of the oven stayed within 5 °C of the temperature indicated by the oven's internal thermometer, a standard guideline used in cell culture practice [50].

Verification was performed by placing the probe of a Fluke thermocouple into a flask in the middle of the oven. The oven was set to 180 °C, and temperature readings were taken using the oven's interface as well as from the thermocouple. Readings were taken every minute during temperature ramp-up, and every five minutes after the target temperature had been reached for a total of one hour at the target temperature. These measurements have been plotted in Figure 3.1.

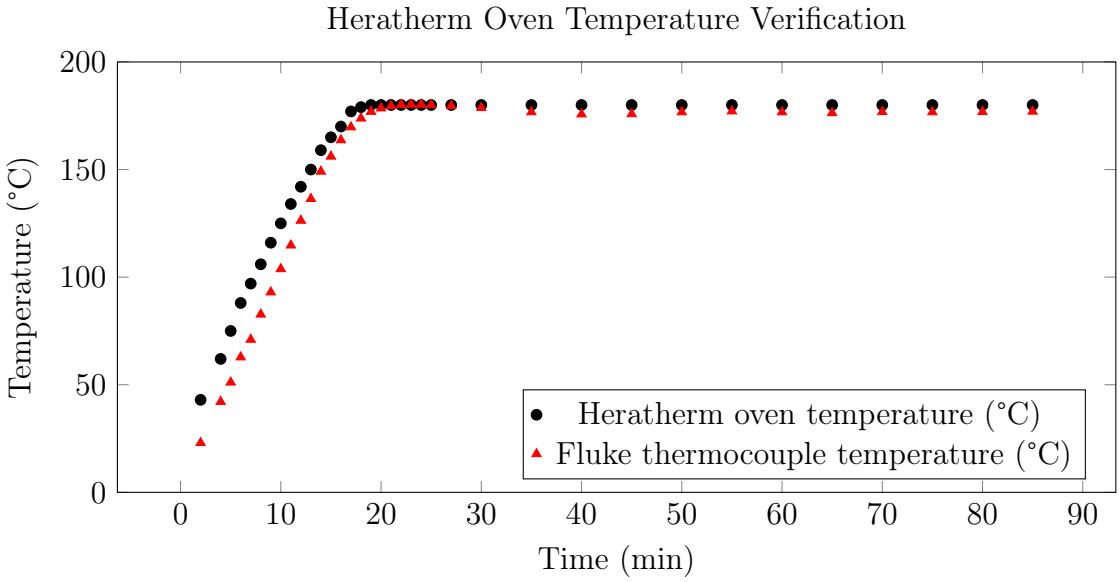

FIGURE 3.1: Temperature profile of the Heratherm dry heat oven as measured by the oven's temperature indicator compared to a thermocouple.

Dynalon™ Kartell Dry heat sterilization indicator tape from Fisher Scientific was also used to verify sterilization conditions. The tape has stripes which change colour to indicate that a high enough temperature has been maintained long enough for

sterilization to occur. Pieces of the tape were placed on beakers to ensure that the colour change would occur under conditions that were verified to have the correct characteristics for sterilization. The colour change of the tape is shown in Figure 3.2.

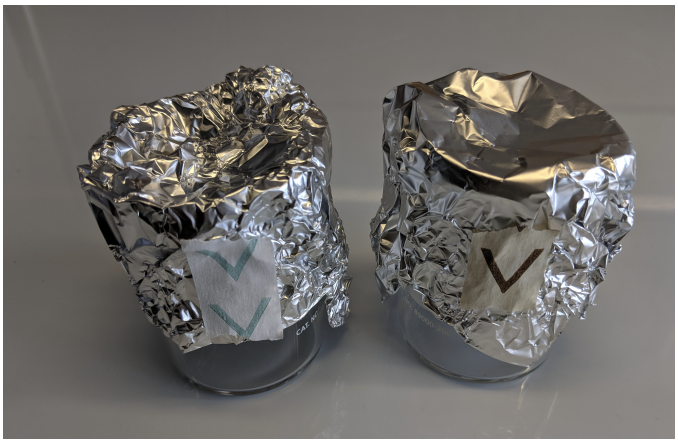

FIGURE 3.2: Beakers with dry heat indicator tape before and after sterilization. The tape on the unsterilized beaker (left) has green stripes, and tape on the sterilized beaker (right) has dark brown stripes.

After the initial temperature verification, routine monitoring was done using indicator tape alone, without secondary temperature monitoring. Tape was placed on every item in the oven during every sterilization.

The parameters assessed in this performance test were the length of the warm-up period, target temperature overshoot, and the difference between load temperature and oven interface temperature. The ranges recommended for sterilization equipment are as follows, and are based on standard recommendations for sterilization ovens used for the purposes of cell culture [50].

- Warm-up time is less than 135 min
- Target temperature overshoot is less than 2 °C
- Temperature of the items in the oven do not deviate more than ± 5 °C

TABLE 3.1: Results of tests for satisfactory sterilizing oven parameters. All tests returned satisfactory results.

Parameter	Recommended Value	Experimental Value	Within Recommended Values?
Warm-up time	$<$ 135 min	22 min	Yes
Overshoot	$<$ 2°C	0.2°C	Yes
Load temperature	$\pm$ 5°C of oven indicator	$\leq$ 4.3°C of oven indicator	Yes

Each parameter verified by this experiment fell within the recommended ranges, and the results are summarized in Table 3.1. The conditions were also sufficient to trigger the colour change in the dry heat sterilization indicator tape. The tape was used in all subsequent sterilizations as an indicator that the oven had reached the expected temperatures.

These results show that the dry heat oven can provide adequate temperatures and consistency over the heating time to sterilize the glassware used in culturing procedures.

3.2 Irradiation Distance & Collimation

3.2.1 Irradiation Setup

A Mini-X X-ray generator from Amptek (Figure 3.3) was used to irradiate lenses. The Mini-X produces low-energy X-rays and supports accelerating voltages from 10 kV to 50 kV and currents from 5 µA to 200 µA [52]. All experiments were done using an accelerating voltage of 40 kV and a current of 99 µA. The voltage of 40 kV was used to avoid potential overheating from running continuously at the highest voltage setting of 50 kV. The current of 99 µA was used because a higher current

would have caused the Mini-X to exceed its maximum specified power output.

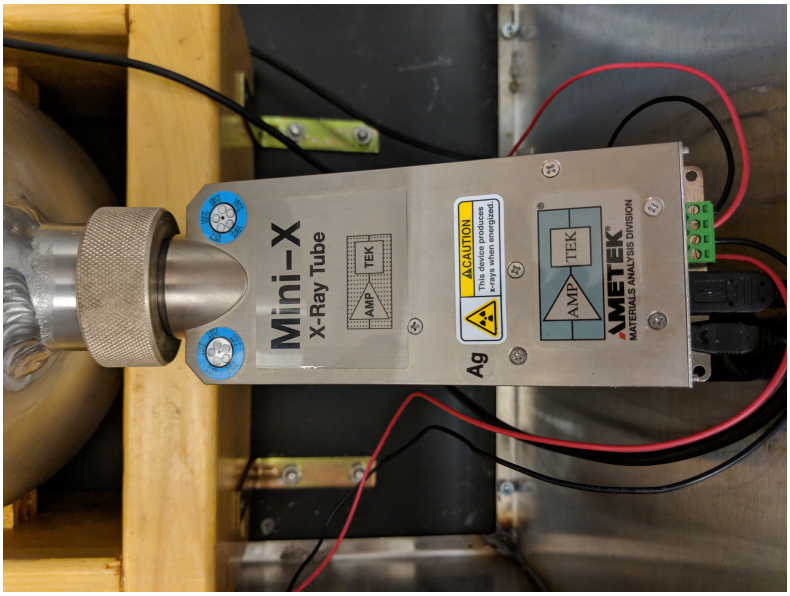

FIGURE 3.3: Amptek Mini-X X-ray generator.

The Mini-X was characterized before beginning lens irradiations in order to evaluate differences in irradiation distance, aperture size, and depth-dose relationships. The characterization of the irradiator consisted of determining which beam spot sizes should be used for lens irradiation (based on distances and collimators), as well as measuring the energy spectrum of the Mini-X to determine the average photon energies seen by the lens.

The Mini-X is housed within an aluminum enclosure, and the targets for irradiation are placed within that enclosure. The setup is shown in Figure 3.4.

3.2.2 Radiochromic Film

Gafchromic™ XR-QA2 radiochromic film from Medron Medical Systems was used to measure beam spot sizes at various distances from the X-ray aperture and with various collimators. This was done to measure beam spot size and uniformity, which were then used to determine the optimal lens position for irradiation.

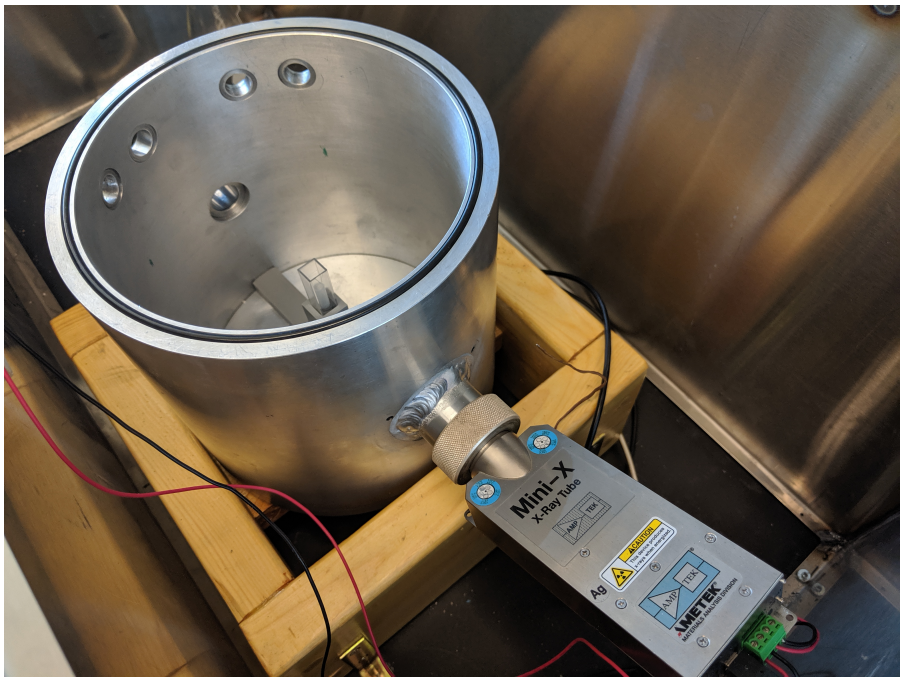

FIGURE 3.4: Setup of the irradiation system.

An insert that could hold a square of film at adjustable distances from the aperture of the irradiator was built for the X-ray irradiator enclosure. This holder was then used to measure the beam spot size at the front, middle, and back of the enclosure to give approximate information about spot sizes at various locations in the enclosure. The front, middle, and back of the enclosure were at distances of about 0.5, 3, and 6 in from the aperture, respectively.

Measurements were then repeated with various collimators, which fit inside the Mini-X aperture and reduce its diameter. This produced an array of beam spot sizes for several combinations of distances and collimators, which were used to determine the optimal irradiation distance; this decision was based on the uniformity of the spot at the various distances from the collimator. The measurements were then repeated at the chosen distance for several collimators, so that the optimal X-ray collimator size could be determined. After initial measurements, a distance for more precise measurements was chosen based on these preliminary results.

The preliminary measurements consisted of determining the spot size at various

distances from the Mini-X aperture: at the far end of the enclosure (6 in), at the middle of the enclosure (3 in), and as close to the aperture as possible (about 0.5 inch). Several collimators were used, with diameters of 3.7 mm, 3.2 mm, 2.5 mm, and 2.0 mm. The diameter of the "open" aperture (i.e. with no collimator) was measured to be 5.6 mm.

The spot size uniformity was assessed by observing the shape and colour of the exposed section of film. The overall beam spot consisted of two slightly offset circles, with the region of overlap being the effective beam spot size. The overlap is consistent in shape and relative size for the various distances and collimators, but is more difficult to distinguish for the smaller spot sizes. The initial batch of films can be seen in Figure 3.5.

The spot sizes seen in the middle of the Mini-X enclosure (i.e., at approximately 3 inches from the aperture) had a slightly more pronounced overlap than at closer distances, but the size of the effective spot formed by the overlap was large enough for the dimensions of the lenses. Therefore, the measurements were repeated using a more precise distance for the middle of the enclosure.

The middle of the enclosure was defined to be 93 mm from the collimator, based on the enclosure's diameter. The spot size measurements were repeated for three different collimators. From the initial measurements (Figure 3.5), using the smaller collimators produced too small of a spot size. Therefore, the three largest collimators were used here. These measurements can be seen in Figure 3.6, and the sizes of the effective beam spots are summarized in Table 3.2.

These measurements led to the decision not to use a collimator for lens irradiation, since the region of overlap seems more clearly defined in the largest spot size. The spot size produced with no additional collimation is also large enough to irradiate a lens and the ion chamber with a uniform field, whereas the spot sizes closer to the aperture or using collimators would not be large enough.

Therefore, the target position for all irradiations was set to be in the middle of the enclosure, 93 mm from the aperture. The X-ray aperture diameter was left as 5.6 mm, which is the size of the machine's aperture with no additional collimation.

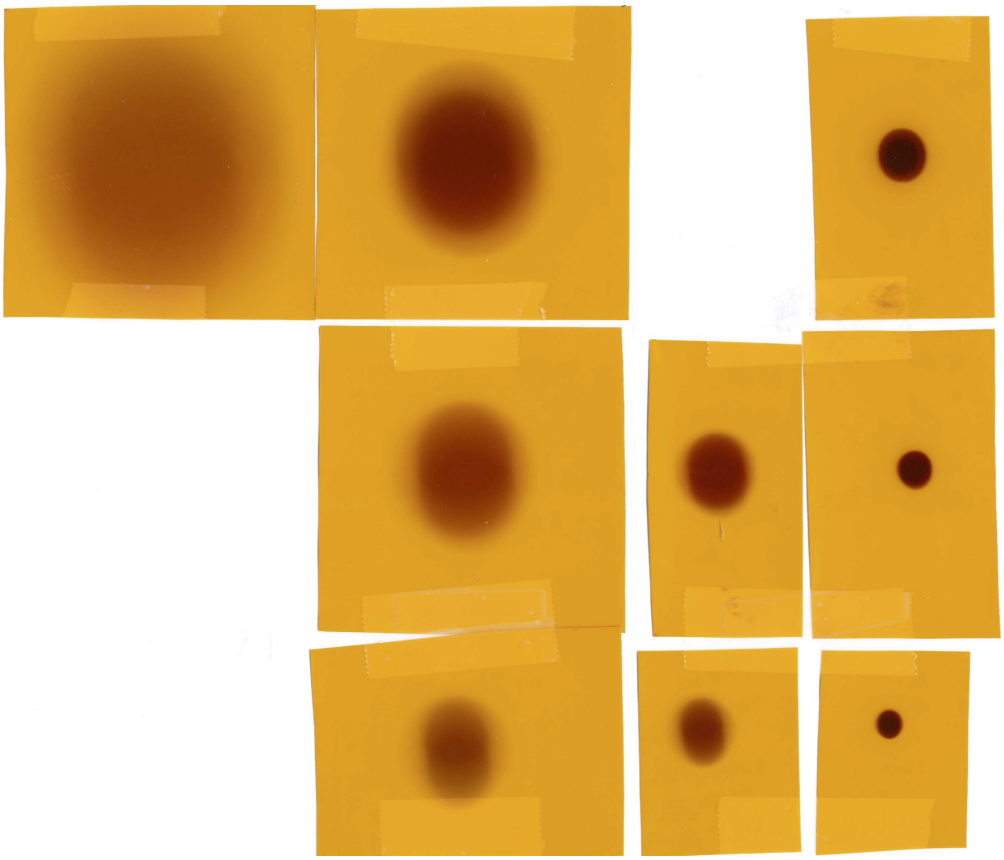

FIGURE 3.5: The initial batch of beam spot sizes measured to assess which distances and collimators were best suited for lens irradiations. Columns, left to right, are distances of 6 in, 3 in, 1.5 in, and 0.5 in from the aperture. Rows from top down are aperture diameters of 5.6 mm, 3.7 mm, and 2.5 mm.

3.2.3 Lens Holder Design

Once an appropriate position for irradiation was determined as described above, a cuvette holder was designed and printed with PLA plastic using a MakerBot™ 3-D printer. The purpose of the holder was to ensure that the cuvette (and thus the lens) was positioned in the same way for each irradiation.

The holder was designed in such a way that it could accommodate either a cuvette or the ionization chamber, and to align all of these in the same way during irradiation. This was to ensure that the ionization chamber would be measuring

TABLE 3.2: Effective spot sizes for various collimators in the middle of the irradiator enclosure at a distance of (93 mm from the aperture).

Collimator Diameter (mm)	Beam Spot Size (mm)
5.6 (no collimator)	30×20
3.7	20×15
3.2	15×10

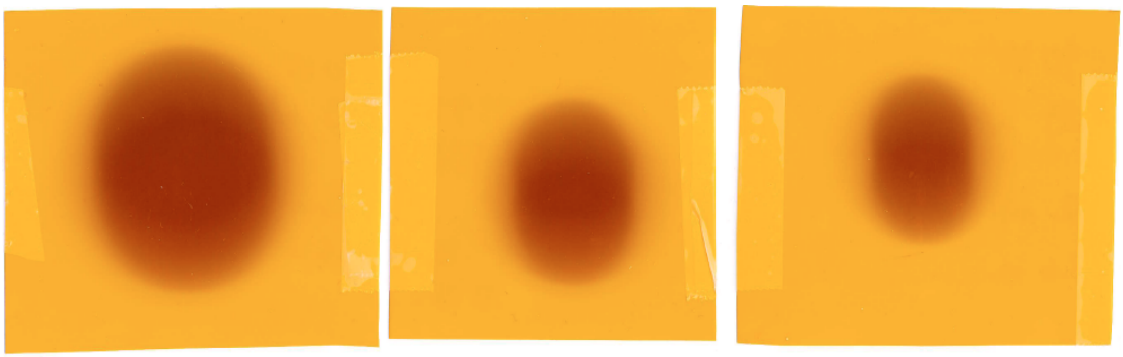

FIGURE 3.6: The radiochromic films from measurements summarized in Table 3.2. Spots were measured at a distance of 93 mm from the aperture, and with collimator diameters of 5.6 mm, 3.7 mm, and 3.2 mm (left to right).

the same X-ray field that the lenses would be exposed to during irradiation. The lens alignment system is shown in Figure 3.7. The printed insert for the holder is shown in more detail in Figure 3.8, for holding the ion chamber (which fits in the circular opening of the second insert, as demonstrated in Figure 3.10).

Figure 3.9 demonstrates how the insert for the ion chamber keeps the window of the chamber exactly in front of the Mini-X aperture, which can be seen as the smallest circle centered in the hole of the insert. The alignment system can be seen in use in Figure 3.10. The insert was designed in such a way to keep the lens and ion chamber centered and at the same height.

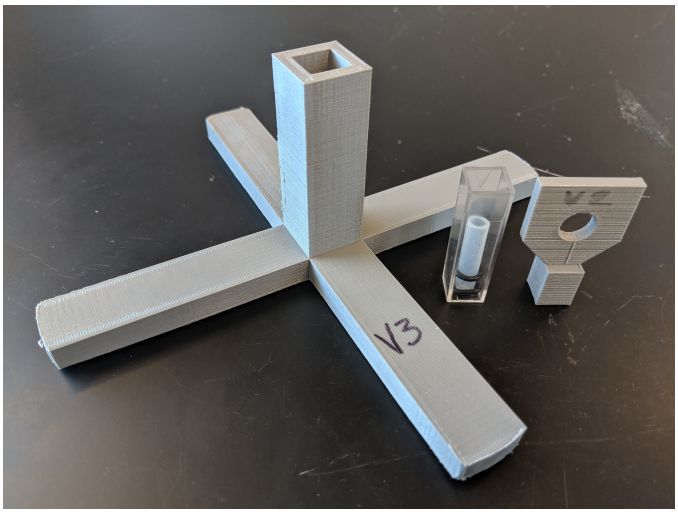

FIGURE 3.7: Alignment system for cuvettes (left) and the ion chamber (right).

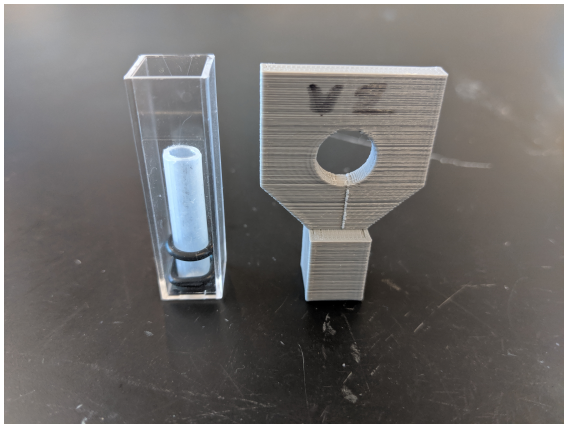

FIGURE 3.8: Two inserts that fit into the lens cuvette holder. One insert is the cuvette that holds a lens for irradiation (left), and one fits the A20 ionization chamber for consistent alignment during dosimetry measurements (right).

3.3 Radiation Characterization & Dosimetry

Radiation measurement and dosimetry for these experiments was mainly done using an ionization chamber. Ionization chambers work by creating an electric field between a cathode and an anode in order to collect the ions produced by ionizing

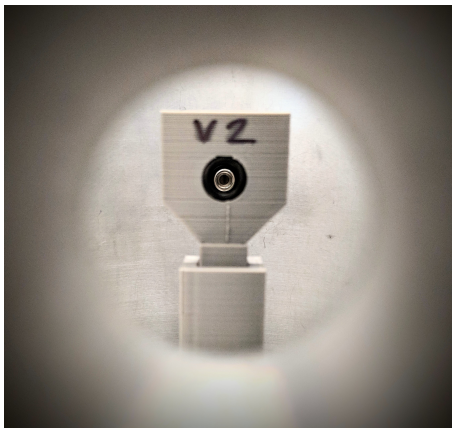

FIGURE 3.9: A demonstration of the alignment provided by the holder and insert system. The insert used here is the ion chamber alignment insert, and the view is from the hole through which the ion chamber is inserted.

radiation. This is measured as a charge, which can then be related to a dose if a calibration factor is known or calculated.

The ionization chamber used in these experiments was a Exradin A20, and was used with aSupermax electrometer, both commercially available from Standard Imaging. The electrometer measures the charge collected by the ionization chamber and uses a system factor to convert collected charge to dose. For all measurements, the ionization chamber was operated at 300 V. Figure 3.10 shows how the ion chamber was set up within the Mini-X enclosure. The window of the ion chamber is the front circular face held by the alignment insert.

3.3.1 Depth-Dose Curve

A depth-dose curve was measured for the Mini-X using the ion chamber. Attenuators of 0.5 mm thick polyethylene terephthalate (PET) were placed in front of the ion chamber, with the total thickness of the plastic ranging from 0.5 mm to 17 mm. The Mini-X was operated at the same settings as would be used for lens irradiation (40 kV, 99 μA). The purpose of these measurements was to determine the dose rates at various thicknesses of attenuator material which simulate the lens

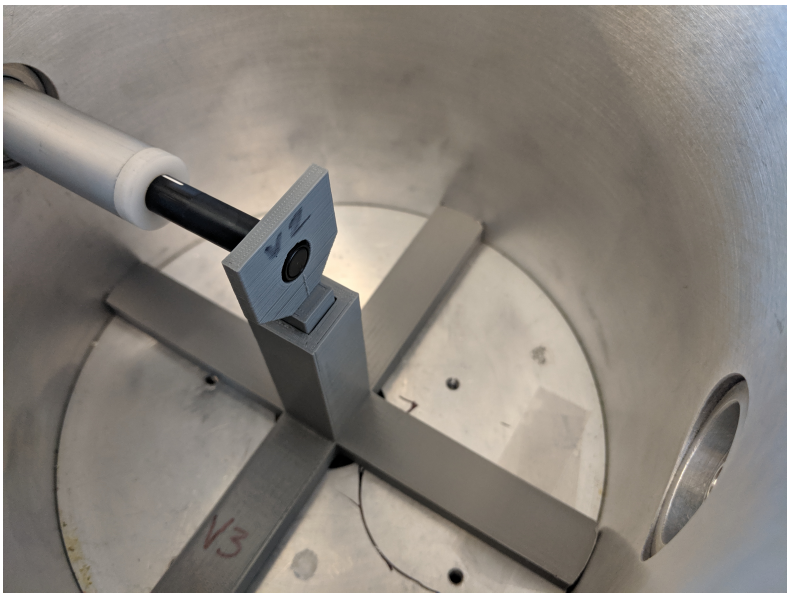

FIGURE 3.10: The Exradin A20 ionization chamber held in alignment with the Mini-X aperture.

tissue. The dose rate measurements through a certain thickness of PET plastic simulate the dose rate through that same thickness of lens tissue. This was done to investigate whether there is a significant change in dose rate across the lens diameter.

The depth-dose curve was measured for the Mini-X at normal operating settings (40 kV and 99 µA). Figure 3.11 shows the results of this measurement. The open dots represent the thickness of PET that corresponds to the diameter of a particularly large lens (6 mm), so virtually all lenses measured experience the dose rates in this section of the curve.

The measured dose rate with 0.5 mm of attenuation is 0.3 Gy/min, and drops below 0.1 Gy/min at 2.5 mm. An average (5 mm diameter) lens would experience a dose rate of about 0.07 Gy/min at its front surface, which would decrease to about 0.03 Gy/min at the back surface.

These measured dose rates were used to calculate the doses that the lenses would experience during their irradiations. Lenses are irradiated in standard polystyrene cuvettes, which are 12 mm wide with 1 mm thick walls. The lens sits centered in

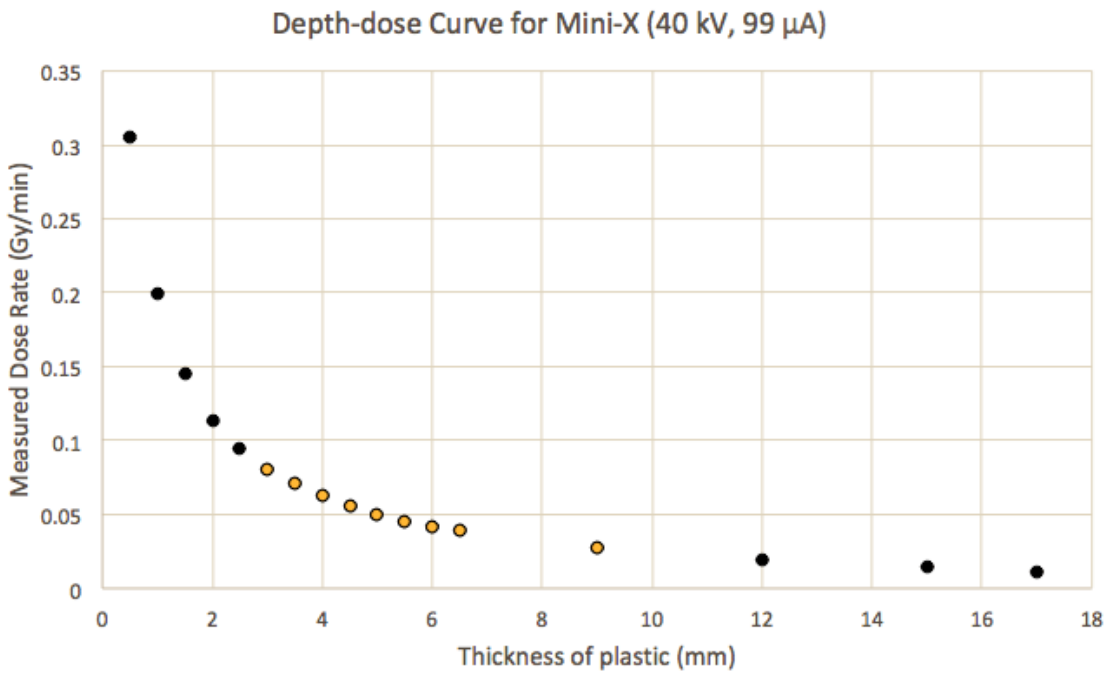

FIGURE 3.11: The depth-dose curve through polyethylene terephthalate measured for the Mini-X X-ray generator set to 40 kV and 99 µA. A lens generally occupies the space between 3.5 mm to 8.5 mm, and thus falls within the region represented by the open points.

the cuvette with its center at a distance of 6 mm from the outside of any of the cuvette's walls. Lenses are generally about 5 mm in diameter and thus occupy the space from approximately 3.5 mm to 8.5 mm as shown in Figure 3.14. Therefore, the dose rates that are used to calculate lens dose are taken from the 3.5 mm to 8.5 mm range of dose rates measured through PET plastic.

The dose to the center of the lens regardless of lens diameter is the dose as measured at a depth of 6 mm. Therefore, the dose rate used to determine irradiation times is 0.04221 Gy/min, which is the dose rate measured through 6 mm of PET. This information was used to determine the irradiation time (total and per fraction) for the lenses at each dose point, all of which are summarized in Table 3.3. These dose values were obtained using the formula shown in Equation 3.1, where D_{lens} is the calculated dose to a given point in the lens, $\dot{D}_{\text{depth}}$ is the dose rate at a particular

thickness of attenuator material corresponding to that point in the lens, and t_{fraction} is the length of one fraction of irradiation time, since lenses were irradiated in four fractions of equal time in order to reduce the effects of decreasing dose rate across the lens diameter.

$$D_{\text{lens}} = \sum \left((\dot{D}_{\text{depth}})(t_{\text{fraction}}) \right) \tag{3.1}$$

The error associated with the dose rate calculated in this way can be calculated from the errors of each dose fraction. The errors in these measurements are error in irradiation time, $\delta t_{\text{fraction}}$, and error in measured dose rate at a particular depth of material, $\delta \dot{D}_{\text{depth}}$. These errors were experimentally determined by calculating the standard deviation across multiple measurements of the same dose rate. The error for a single dose fraction, $\delta D_{\text{fraction}}$, can be calculated by propagating these errors and is shown in Equation 3.2. The total error in one dose calculation for a lens is then given in Equation 3.3.

$$\delta D_{\text{fraction}} = D_{\text{fraction}} \sqrt{\left(\frac{\delta \dot{D}_{\text{depth}}}{\dot{D}_{\text{depth}}} \right)^2 + \left(\frac{\delta t_{\text{fraction}}}{t_{\text{fraction}}} \right)^2} \tag{3.2}$$

$$\delta D_{\text{total}} = \sqrt{(\delta D_{\text{fraction 1}})^2 + (\delta D_{\text{fraction 2}})^2 + (\delta D_{\text{fraction 3}})^2 + (\delta D_{\text{fraction 4}})^2} \tag{3.3}$$

For calculating dose to the lens core, the dose rates for each fraction are the same (as simulated by 6 mm of PET plastic). However, these equations can also be used to account for differences in dose rates when calculating the dose to a point elsewhere in the lens. For example, the depth-dose data can also be used to approximate the difference between dose to the lens core and dose to a given point on the periphery. Since lenses were irradiated in four fractions with the cuvette being turned one quarter turn between fractions, the point on the surface of the lens that is closest to the X-ray aperture first experiences one irradiation fraction at one particular dose rate (as measured at about 3.5 mm of PET plastic). During the next fraction,

that point on the lens rotates around the center and experiences another fraction of time in a dose rate as measured at 6 mm of PET plastic. The lens then turns again and the point is at its furthest from the X-ray aperture, where it experiences a dose rate as measured at 8.5 mm of PET plastic. Finally, during the fourth fraction, the point experiences the 6 mm dose rate again. This is described by Equation 3.4.

$$
\begin{aligned}
D_{\text{surface}} &= \left(\dot{D}_{3.5\text{mm}} + 2\dot{D}_{6\text{mm}} + \dot{D}_{8.5\text{mm}}\right)(t_{\text{fraction}}) \qquad (3.4)\\
D_{\text{surface}} &= (0.0712\ \text{Gy/min} + 2(0.0442\ \text{Gy/min}) + 0.0276\ \text{Gy/min})\,(t_{\text{fraction}})\\
D_{\text{surface}} &= (0.183\ \text{Gy/min})\,(t_{\text{fraction}})
\end{aligned}
$$

The results of dose calculations and error analysis based on the set of equations presented above (Equations 3.1 to 3.4) are sumamrized in Table 3.3.

TABLE 3.3: Irradiation times and their corresponding lens core and lens surface doses for several points up to 2 Gy.

Total Irradiation Time (s)	Irradiation Time per Fraction (s)	Dose to lens core (Gy)	Dose to lens surface (Gy)
3000 ± 2	750 ± 1	2.210 ± 0.002	2.339 ± 0.003
1500 ± 2	375 ± 1	1.105 ± 0.002	1.170 ± 0.002
510 ± 2	128 ± 1	0.337 ± 0.002	0.399 ± 0.002
405 ± 2	101 ± 1	0.298 ± 0.001	0.315 ± 0.002
252 ± 2	63 ± 1	0.186 ± 0.001	0.196 ± 0.002
120 ± 2	30 ± 1	0.088 ± 0.001	0.094 ± 0.002
60 ± 2	15 ± 1	0.044 ± 0.001	0.047 ± 0.002

Calculating the surface dose in this way demonstrates that the periphery of the lenses receives a higher dose than the lens core. This is due to the non-linear decrease in dose rates across the diameter of the lens. The surface of the lens could be receiving as much as 1.75 times the dose rate that the core gets (in the case

of a typical 5 mm diameter lens). This ratio increases towards 2 times the dose rate for the surfaces of larger lenses where the dose rate can reach 0.08 Gy/min at the lens surface. Table 3.3 also includes the calculated surface dose compared to the dose calculated for the core of the lens for each of the dose points in the lens irradiations.

The results of the depth-dose measurements show that there is a decrease in dose rate across the diameter of the lens from the spectrum hardening as it passes through the attenuator material. The next experiment (discussed in Section 3.3.2) addresses the question of whether the expected increase in average photon energy associated with spectrum hardening necessitates the use of correction factors for calculating lens dose.

Though dose rates do decrease over the diameter of the lens, they are more consistent across this distance than they are over the first several millimetres of attenuating material (i.e. through the cuvette wall and culture medium). It is desirable for the significant decrease in dose rate to occur in the material in front of the lens rather than across the lens itself, since this means that the decrease in dose rate through the lens will be less drastic. While this does not entirely eliminate the difference in dose to the front vs. the back of the lens, it is less of a difference than if there was less filtering material.

Overall, the depth-dose measurements allow for the comparison of dose to the lens core compared to the lens surface. Though this difference is relatively small, it is important to consider during dosimetry, so that there is an understanding that the periphery of the lenses has received a higher dose than the core.

3.3.2 Lens Dose vs. Air Kerma

The ion chamber measures air kerma (the kinetic energy released per unit mass of air) by collecting the charge from ionized particles and using a calibration factor to convert this charge to a kerma value. The air kerma calibration factor for the Exradin A20 ion chamber is 3.8×10^8 Gy/C [53].

Under conditions of charged particle equilibrium, the measured air kerma represents the dose imparted to air. However, the objective of this work is to investigate dose effects in eye lenses. An assessment was performed in order to determine whether there is a significant difference between dose to air and dose to eye lens tissue at the photon energies being used in these irradiations, and whether a correction factor was necessary for dosimetry.

The correction factor is calculated as the ratio of the mass energy-absorption coefficients for the eye lens tissue to that of air. Multiplying this ratio by the measured dose to the air (i.e., the air kerma) adjusts the measured air dose to theoretical lens dose. This relationship is shown in Equation 3.5.

$$D_{lens} = D_{air} \times \frac{(\mu/\rho)_{\text{lens}}}{(\mu/\rho)_{\text{air}}} \tag{3.5}$$

However, the mass energy-absorption coefficient changes with photon energy, and thus the mass energy-absorption coefficient must therefore be represented as the normalized sum of the coefficients at each energy multiplied by the photon energy fluence at that energy, as shown in Equation 3.6.

$$\overline{(\mu_{en}/\rho)} = \frac{\sum \Big((\mu/\rho)_E \times E \times P(E) \Big)}{\sum \Big(E \times P(E) \Big)} \tag{3.6}$$

The National Institute of Standards and Technology (NIST) provides mass energy-absorption coefficients for both air and eye lens tissue [54]. This data was used to calculate the effective $(\mu/\rho)_{\text{lens}}$ values for the lens using the equations above. This process is described in the following sections, since it involves measuring the photon energy distribution spectra for the lens.

X-123 Calibration

In order to measure the photon distribution spectra across the lens, a commercially available Amptek™ X-123 low-energy X-ray spectrometer (Figure 3.12) was first

calibrated for the photon energy range of interest.

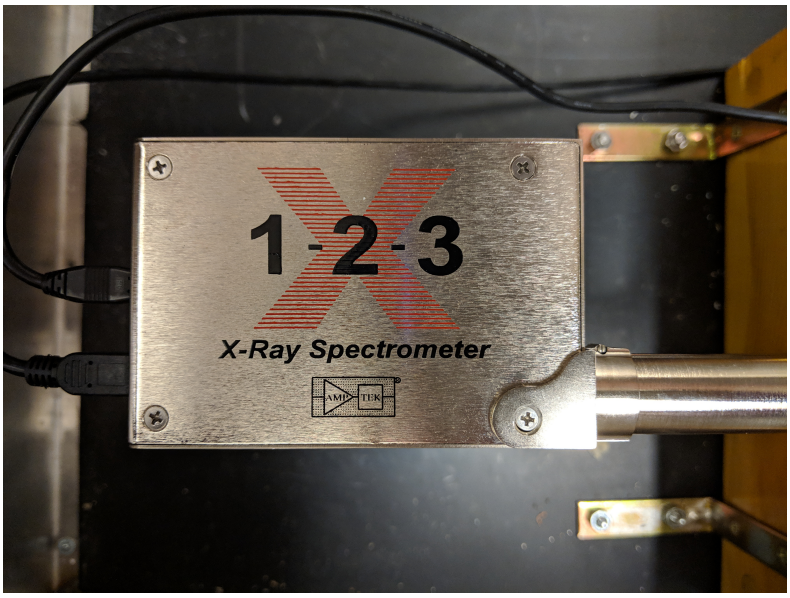

FIGURE 3.12: Amptek X-123 X-ray Spectrometer.

The spectrometer was calibrated using Am-241 and Fe-55 sources, which provided six suitable peaks all together. The characteristic X-rays from the silver target of the Mini-X were also used for the calibration, for a total of eight peaks, as shown in Table 3.4. All of these peaks have energies below 60 keV and are thus suitable for low-energy calibration of the range of energies expected for the 40 kV Mini-X.

Figure 3.13 shows the resulting calibration curve produced for the X-123. The calibration equation produced by fitting a line through all of the data points was used to calibrate the raw spectrum data from the X-123 spectrometer. The spectrometer was then used to measure the photon distribution spectra from the Mini-X for various attenuator thicknesses.

The purpose of calibrating the spectrometer was to measure the photon energy distribution spectra as experienced by a lens. In general, photon energy distribution spectra for increasing attenuator thicknesses show that lower-energy photons are filtered out, thereby decreasing the overall number of photons reaching the target, but increasing the average photon energy. The front of a lens should, therefore, be subject to a higher dose rate from a larger number of photons, but with a lower

TABLE 3.4: The eight usable energy peaks provided by Am-241, Fe-55, and the Ag target for calibration of the X-123 low-energy X-ray spectrometer.

Source	Energy (keV)
Am-241	59.5
	26.3
	13.8
	17.71
	21.0
Fe-55	5.9
Ag	22.16
	24.9

average energy compared to the back of the lens. The back of the lens would experience a comparatively lower dose rate from a lower number of photons, but a higher average photon energy. As previously described, mass energy-absorption coefficients (μ_{en}/ρ values) are used to relate the measured dose to air and the corresponding dose to the lens (Equation 3.5). However, the change in dose rate across the lens diameter due to spectrum hardening suggests that there is a change in average photon energy for different parts of the lens, and it follows that there is also a change in lens-to-air ratio of the mass energy-absorption coefficients. Therefore, the photon energy distribution spectrum was measured for the front, middle, and back of the lens in order to calculate and compare changes in effective mass energy-absorption coefficients across the lens.

X-Ray Distribution Spectrometry

The purpose of measuring the photon distribution spectra was to determine the extent of the differences in photon distribution across the diameter of the lens. The spectrum data was also used to calculate separate $(\mu/\rho)_{\text{lens}}$ values for different points across the lens diameter.

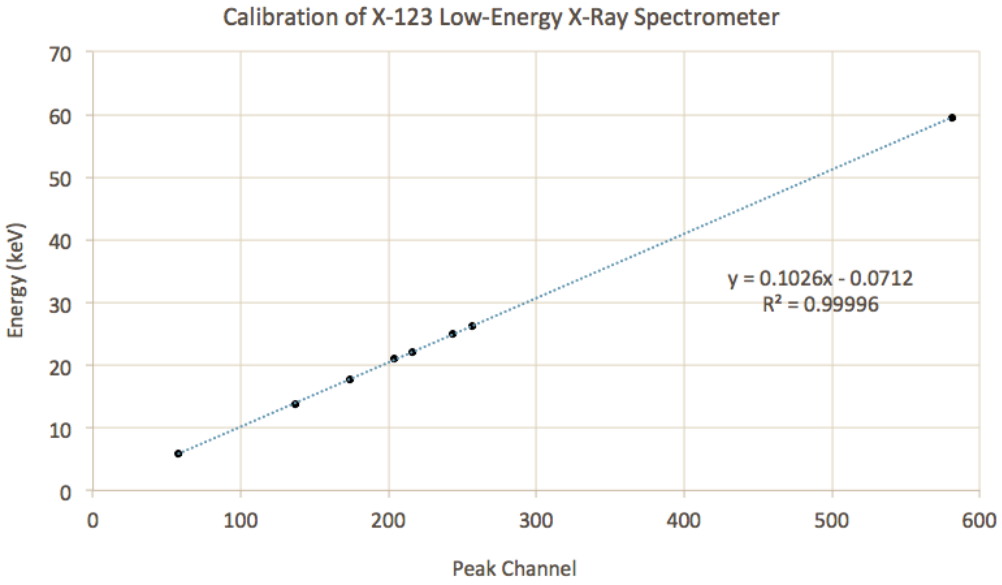

FIGURE 3.13: The calibration data for the X-123 spectrometer using low-energy sources.

These measurements were taken by simulating the amount of material that X-rays pass through before reaching the front, middle, or back of a lens, as shown in Figure 3.14 for a typical 5 mm diameter lens. The thickness of polyethylene terephthalate (PET plastic) corresponding to the amount of material and lens tissue in front of a particular part of the lens was placed in front of the spectrometer's window, and the Mini-X was set to the same voltage as during lens irradiation (40 kV). The current was lowered to 5 µA because the spectrometer was saturated by the usual 99 µA that is used for lens irradiation. Lowering the current reduces the number of photons reaching the spectrometer, but the energy distribution of the photons remains the same.

The spectrometer was irradiated with 3.5 mm of PET in front of the window to measure the X-ray energy spectrum that would be seen by the front of the lens. 6 mm of PET was used for the middle of the lens, and 8.5 mm for the back of the lens.

The spectra measured for the front, middle, and back of the lens were then normalized to show the probability $P(E)$ that a photon would have a particular energy E.

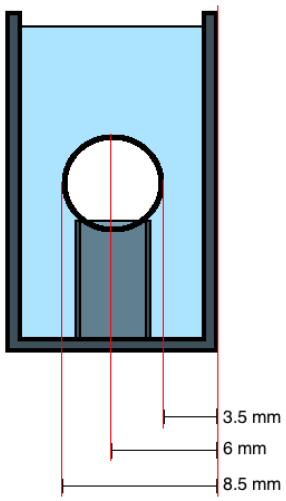

FIGURE 3.14: A schematic showing the thickness of material (polystyrene cuvette (grey) and culture medium (blue)) in front of the lens (white), which sits on a plastic stand. There is 3.5 mm to the front of the lens, 6 mm to the middle, and 8.5 mm to the back.

These probabilities were then multiplied by the respective mass energy-absorption coefficient $(\mu/\rho)_{\text{lens}}$. These values were then summed to give an effective mass energy-absorption coefficient for the given photon spectrum, as described in Equations 3.5 and 3.6.

Figure 3.15 shows the results of the photon energy spectrum distribution measurements. The spectra are shown as normalized probability distributions, with each point representing the probability $P(E)$ that a photon from the Mini-X has a particular energy E. There is noticeable spectrum hardening occurring: as the spectrum is attenuated, there is a decrease in total number of photons reaching the spectrometer, but an increase in peak energy. The peak energy at the front of the lens is approximately 13 keV, which increases to about 16 keV towards the back of the lens. The sharp peaks in the spectra (at about 22 keV and 25 keV) are the characteristic X-rays from the silver target in the Mini-X. These peaks are at the same position for each spectrum, confirming that the energy differences in the bremmstrahlung portion of the spectrum do represent actual differences and are not simply artifacts of imprecise measurements.

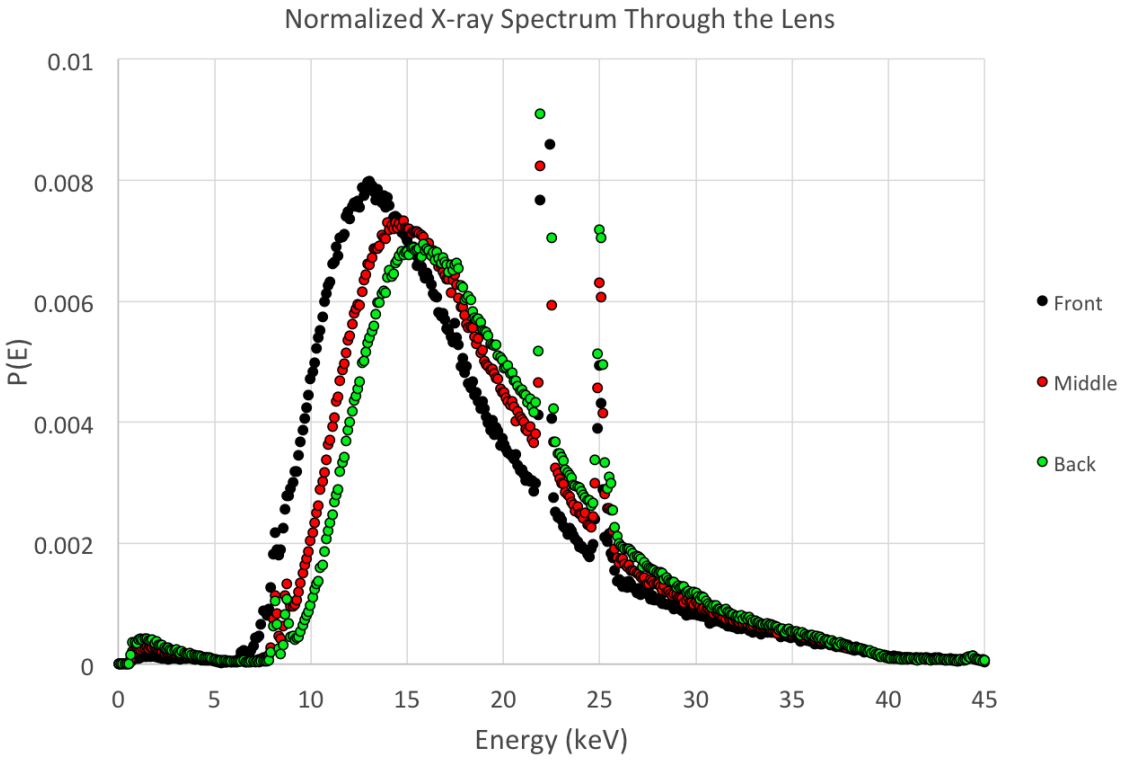

FIGURE 3.15: The normalized probabilities of X-ray energies reaching the front, middle, and back of the lens. The front of the lens experiences a slightly lower average X-ray energy (∼13 keV) than the back of the lens (∼16 keV).

Mass energy-absorption coefficients (μ_{en}/ρ values) for air and lens tissue were obtained from NIST [54] and plotted to show the change for different photon energies, as shown in Figure 3.16.

Mass energy-absorption coefficients are only given for certain energies in the 0 - 60 keV range, and are represented by the points in the plot in Figure 3.16. The values are very similar for air and lens tissue, though air has slightly higher values (these differences are demonstrated in Table 3.5 for selected photon energies). Curves were fitted to both sets of points, and the equations of these curves were used to approximate the μ_{en}/ρ values for the energies between the given points. This provided a μ_{en}/ρ value for both air and lens tissue for every energy measured by the X-123 spectrometer. These values were then used in the equation relating dose to

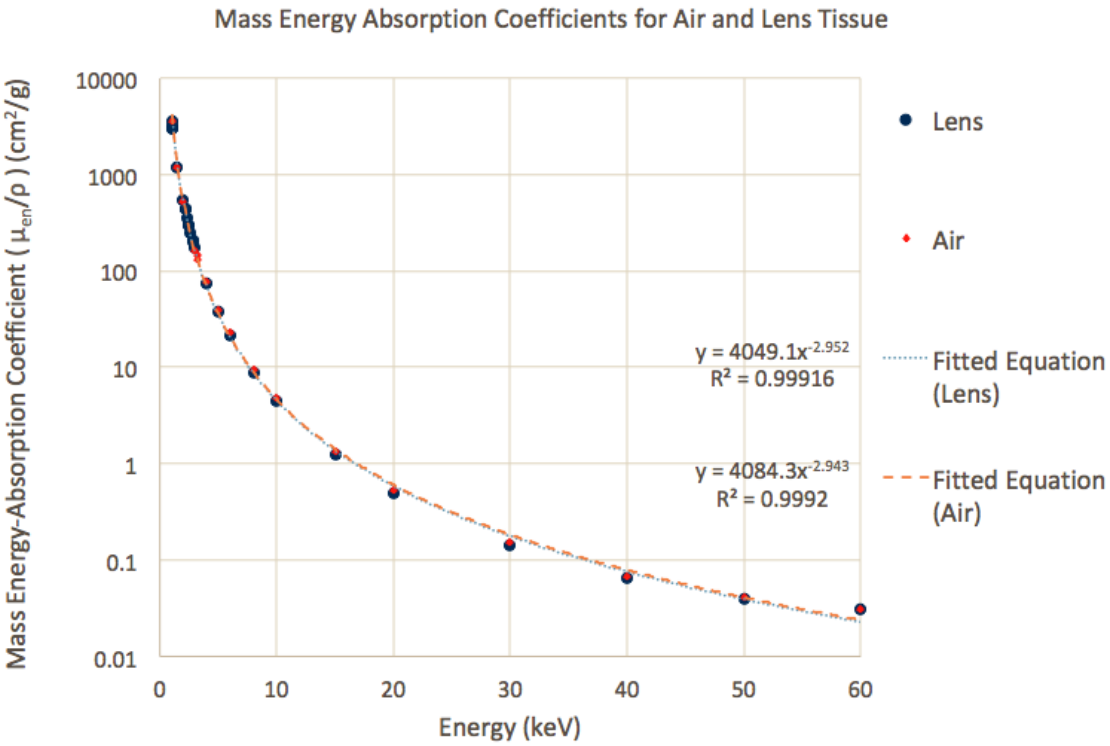

FIGURE 3.16: Mass energy-absorption coefficients for both air and lens tissue for the range of energies expected from the Mini-X.

air and dose to lens tissue using the ratio of μ_{en}/ρ values for the two materials (as previously described by Equations 3.5 and 3.6). This was done for each spectrum measured, representing the front, middle, and back of the lens. The results of these calculations are summarized in Table 3.6.

The ratio of lens-to-air μ_{en}/ρ values for the front-of-lens spectrum is 0.974. The ratios for the middle and back of the lens are 0.978 and 0.981 respectively.

The back of the lens has the highest effective μ_{en}/ρ value, with 37.99 cm^2/g for lens tissue and 38.73 cm^2/g for air. The back of the lens also has the highest lens-to-air μ_{en}/ρ ratio of 0.981. The front of the lens has the lowest μ_{en}/ρ values, with 27.88 cm^2/g for lens tissue and 28.63 cm^2/g for air, and also has the lowest lens-to-air ratio of 0.974. The higher effective μ_{en}/ρ coefficients for the back of the lens can be explained by the small peak of very low-energy photons (1.5 keV) that is present in all three spectra (Figure 3.15), but is largest for the back-of-lens

TABLE 3.5: A comparison of mass energy-attenuation coefficients for air and lens tissue. For all energies shown here, the coefficients for air are slightly higher than for lens tissue. The differences are largest in the 10 keV to 40 keV range.

Energy	μ_{en}/ρ (Lens) (cm^2/g)	μ_{en}/ρ (Air) (cm^2/g)	Percent Difference
1 keV	3590	3600	0.29
10 keV	4.46	4.74	6.09
20 keV	0.499	0.539	7.71
30 keV	0.142	0.154	8.11
40 keV	0.0642	0.0683	6.19
50 keV	0.0396	0.0410	3.47

spectrum. This peak is smaller for the middle of the lens, and smaller still for the front of the lens. Though these energies make up a relatively small proportion of all photons reaching the lens, the μ_{en}/ρ coefficient at very low energies is very high: around 3600 cm^2/g at 1 keV, which is 800 times as large as the 10 keV μ_{en}/ρ value. Since the effective μ_{en}/ρ value is a weighted average for the normalized photon distribution spectrum, the very high μ_{en}/ρ values for very low energies result in a significantly higher effective μ_{en}/ρ value for the spectra with slightly larger proportion of very low-energy photons.

This is also a possible explanation for the ratio of weighted lens-to-air μ_{en}/ρ values being closest to unity towards the back of the lens. The very low-energy photons (around 1.5 keV) have the smallest percent difference between μ_{en}/ρ values for lens tissue vs. air (0.29%, as shown in Table 3.5, compared with up to 8% at 30 keV). Since the most heavily weighted μ_{en}/ρ values are those with the closest lens-to-air agreement, this leads to the back-of-lens spectrum to have a lens-to-air μ_{en}/ρ ratio closest to unity.

However, if the objective of these calculations is to determine the effect of the

TABLE 3.6: A comparison of the calculated energy-weighted lens-to-air $\overline{\mu_{en}/\rho}$ values (derived from Equation 3.6) (in cm^2/g) and ratios for the front, middle, and back of a lens, for the spectra including and excluding the 1.5 keV peak.

Full Spectrum Data			
	$\overline{\mu_{en}/\rho}$ (Lens)	$\overline{\mu_{en}/\rho}$ (Air)	Ratio
Front of lens	27.88	28.63	0.974
Middle of lens	31.96	32.68	0.978
Back of lens	37.99	38.73	0.981

Spectrum Data Excluding 1.5 keV Peak			
	$\overline{\mu_{en}/\rho}$ (Lens)	$\overline{\mu_{en}/\rho}$ (Air)	Ratio
Front of lens	21.25	21.94	0.968
Middle of lens	17.23	17.81	0.968
Back of lens	15.43	15.95	0.967

shifting bremmstrahlung spectrum on μ_{en}/ρ ratios, then the 1.5 keV peak can be excluded. The results of removing this peak show that there is an overall decrease in mass-energy transfer coefficients from the front to the back of the lens (from 1.67 cm^2/g to 1.03 cm^2/g), which is consistent with the average photon energy increasing over this distance. However, the ratios of lens-to-air dose remain consistent for the front, middle, and back of the lens (the ratio is 0.97 in all cases). This is also summarized in Table 3.6.

Overall, these measurements have shown that there is a measurable difference between the dose to air (as measured by the ion chamber) and the dose to lens tissue, with the ratio of lens-to-air μ_{en}/ρ values ranging from 0.987 to 0.992 across the lens diameter. This could be important to address for potential future experiments with more precise dosimetry, but for the purposes of this work, it is sufficient to consider the dose measured by the ion chamber to be representative of the dose to the lens itself.

Chapter 4

Eye-Lens Irradiation Experiments

4.1 Dissection & Culturing Methods

4.1.1 Aseptic Technique

Aseptic technique refers to performing dissection and culturing in a way that does not introduce biological contaminants into cultured cells, tissues, or organs. There are several satisfactory methods of maintaining sterility during preparation of culture media and while performing culturing procedures. Methods used in these experiments are described in the following sections, and were generally chosen based on availability of equipment and instruments as well as suitability for the volume of work being performed.

Dissection was done partially on the benchtop without aseptic procedures when the dissection was non-sterile (when handling the fish heads or whole eyeballs, which had already been exposed to the environment), and partly under sterile (aseptic) conditions using sterile labware. All culturing was also performed under sterile conditions.

Flow Hood for Aseptic Work

Sterile handling of lenses was done inside a laminar flow hood (LFH). Generally, sterile culturing work is done in a biological safety cabinet (BSC), not an LFH, since

a BSC's primary purpose is to protect the operator from pathogens in the material being cultured [17]. This was not necessary for the experiments in this work, since the lenses were from fish meant for human consumption and thus no pathogens or other biological safety concerns were present. Therefore, an LFH was sufficient for this work, as the primary purpose of the LFH is to provide sterile conditions for the contents of the hood, rather than to provide sterile conditions for the operator. The LFH was kept empty, apart from the sterile glassware and instruments used for dissection and culture medium changes. Keeping the LFH empty allows for proper air flow within the hood, which ensures that sterile conditions are maintained.

The surface inside the laminar flow hood was swabbed with 70 % alcohol before every use, during use when moving new items to the work area, and after use when items had been returned to their usual place. All containers with sterile contents were only ever opened and transferred inside the laminar flow hood. While containers with sterile contents could be opened and held vertically in laminar flow (which is not good practice on an open bench), nothing should come into the space between the HEPA filters at the top of the hood and the open container (including hands). Pouring sterile contents from nonsterile containers produces the possibility of contamination, and therefore all sterile contents were transferred using sterile pipettes. These techniques are all considered to be essential or general good practice in cell culture [17] [50] [55].

4.1.2 Dissection and Sample Preparation

The rainbow trout (*Onchorhynchus mykiss*) used in these experiments were obtained from Linwood Acres Trout Farm in Campbellcroft, Ontario, approximately 40 min away from UOIT by car. Fish heads were removed by site staff and transported on ice to the UOIT laboratory.

Eyeballs were removed from all fish heads by using fine-point dissection scissors to sever the eyeball from the surrounding connective tissue and from the optic nerve at the back of the eye. Excised eyeballs were kept in a Petri dish on ice (Figure 4.1) until all eyes were removed from all fish.

FIGURE 4.1: Eyeballs were excised from all fish and kept on ice until lens excision began.

Once all eyeballs were removed, the dissection was moved to sterile conditions in the laminar flow hood. To remove the contents from each eyeball, an incision was made along the equator of the sclera. By holding the eyeball incision-side down over a sterile Petri dish filled with H-10 culture medium (see section 4.1.3) and applying light pressure to the opposite side of the eyeball, the contents were gently squeezed out without making contact with any dissection instruments, shown in Figure 4.2.

The lenses were then cleaned by separating them from the surrounding vitreous body (a clear gel throughout the eyeball) and choroid (a black film inside the posterior surface of the sclera). The vitreous body is a clear gel-like substance and can be removed by grasping it with fine-point dissection forceps while preventing the lens from moving using a flat, blunt tool such as a scoopula. Pieces of choroid can be removed in a similar manner, since choroid often sticks to small pieces of vitreous body rather than to the lens. The lenses can generally be cleaned without having to bring sharp instruments into contact with the lenses themselves. The

FIGURE 4.2: Removing the eyeball contents without touching the lens with dissection instruments.

exceptions are pieces of choroid that stick to the lens itself; these can be removed by using the flat sides of fine forceps to grasp the choroid piece. Pieces of choroid that are not on the equator of the lens can be left attached if they are small, since they will not interfere with the laser measurement system which only examines the diameter of the lens across its equator.

When removing the vitreous body, it is helpful to leave attached the retractor lentis muscle or ligament that holds the lens within the eyeball. This can serve as a handle with which to move the lens between containers without having to touch the lens itself with instruments.

Lens cleaning was done in two stages to maintain relatively clean medium and prevent the cleaning process from being hindered by larger pieces of removed tissue. Three standard Petri dishes were used for lens cleaning. Large pieces of choroid and vitreous body were removed in the first Petri dish and the partially cleaned lens was moved into clean medium in a second dish, where the smaller pieces of vitreous body and choroid were removed. The fully cleaned lenses were kept in a third clean dish until the procedure was complete for all lenses. The stages of this

cleaning process are shown in Figure 4.3.

FIGURE 4.3: The stages of the lens cleaning process: the far Petri dish shows empty sclera, the middle dish shows removed pieces of choroid and vitreous body, and the closest dish shows cleaned lenses.

Cleaned lenses were placed into the wells of a sterile, non-tissue treated 24-well plate (shown in Figure 4.4) and covered with H-10 medium for culturing. Plates were labelled and placed into a refrigerator kept at 10 °C. Medium was changed every 24-48 h using sterile syringes, as described in Section 4.1.3.

4.1.3 Culturing Methods

The culture medium used in these experiments was H-10 fish lens culture medium, which has been used successfully in fish eye lens culturing experiments in the literature [13] [23] [30] [31].

H-10 culture medium was created in the laboratorty from its constituents as reported in the literature, and was composed of 135.5 mM NaCl (Thermo Fisher),

FIGURE 4.4: A 24-well plate, used to house lenses during culturing.

5.0 mM KCl (Thermo Fisher), 2.0 mM $CaCl_2$ (VWR), 5.0 mM glucose (VWR), and 10.0 mM HEPES physiological pH buffer (Thermo Fisher), with 100 u/mL penicillin and 100 µg/mL streptomycin (Thermo Fisher). Medium was prepared using Type I ultrapure (tissue culture grade) water and kept under the same refrigeration as lenses in culture to minimize temperature changes for the lenses during culture medium changes.

Medium was prepared in 500 mL batches by using sterile glassware to add appropriate amounts of each constituent to a sterile flask, then by filling the flask to 500 mL with tissue culture grade water.

The culture medium was changed every 24-48 h. To change the medium, the old medium was first removed from the well using a sterile dropper. A sterile syringe was then filled with fresh culture medium, and a 0.2 µm polyethersulfone (PES) filter was attached to the syringe to sterilize the medium. This was done to provide a second measure of medium sterilization immediately prior to use. The fresh, sterile medium was then added directly to the wells. This process took approximately two minutes to complete for a full 24-well plate, and thus the lenses did not experience a significant temperature change from being outside of the chilled culture environment.

4.2 Lens Focal Capacity Analysis

4.2.1 Laser Focal Analysis Apparatus

Laser focal analysis was used in these experiments to quantify changes in the refractive capacity of the lenses. The system built and used here was based on an automated laser scanning system built by Weerheim and Sivak [25].

A basic laser scanning system was built by securing a 5 mW laser to a 25 µm-incremented slide table. A collimator was fitted to the laser to reduce the beam to a 0.15 mm diameter at the aperture. A millimetre-grid was used as a screen onto which the laser beam was projected. The screen was placed far enough away from the lens position that small angles of refraction would be easily visible as relatively large changes in position on the grid, and close enough to the laser aperture to minimize beam spread. A cuvette was used as a lens container (as shown in Figure 3.14) and was placed between the laser and the screen. Figure 4.5 shows the basic schematic of the system, and Figure 4.6 shows the final experimental setup.

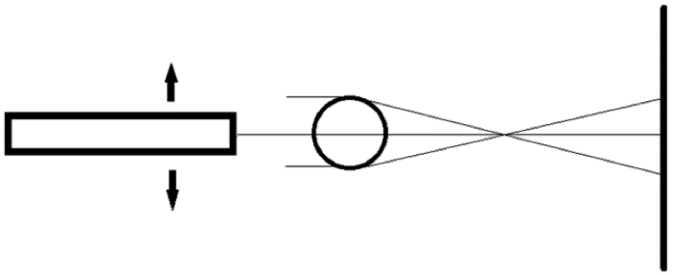

FIGURE 4.5: A schematic of the laser system used in lens analysis. A laser (left) shines a beam of light through a lens (middle), which refracts the beam onto the screen (right). The focal point can be graphically shown by superimposing the paths of several beams through a lens.

4.2.2 Focal Analysis Methods

Focal analysis was performed by moving the laser beam in 0.13 mm steps across the lens and noting where the beam fell on the screen at each step. One data point

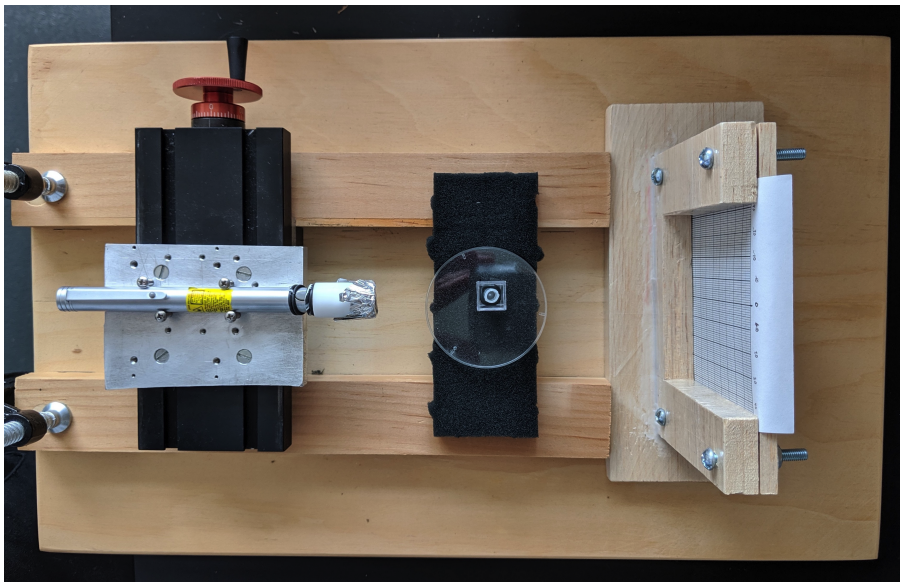

FIGURE 4.6: The laser system used in lens focal analysis. The laser (left), mounted on a slide table, sends beams through a lens in a cuvette (center). The beams are refracted and fall onto the screen (right).

consists of two sets of coordinates, giving the relationship between where the beam passes through the lens and where it falls on the screen. The data for a single lens scan (i.e., all beams across the diameter for a given day) includes information for approximately 30 beams, depending on the diameter and condition of the lens. This data can be represented qualitatively by creating a focal profile, or quantitatively by calculating back vertex distance (BVD) and focal length variability (FLV). The methods for calculating these values are described in the following sections.

Focal Profiles

The full data set for one lens during one set of measurements is plotted to illustrate the beam paths superimposed on one another; this produces a visual representation of the focusing capacity of the lens. An example of a focal profile for a healthy lens is shown in Figure 4.7. This method of displaying focal length data is useful for assessing the overall quality of the lens and understanding, conceptually, the effect

that changes in refraction have on the lens' overall focusing ability.

In these profiles, the left vertical axis is the eccentricity of each beam that is sent through the lens. The right vertical axis is the position on the screen where the beams fall. One data point is represented by one line which connects the position a particular beam enters the lens (i.e., the height on the left vertical axis) to the position the beam falls on the screen (the height on the right vertical axis).

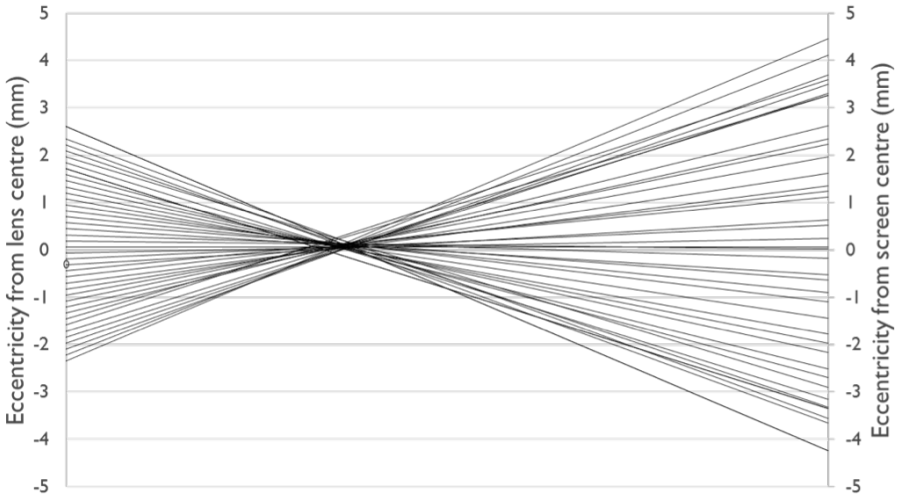

FIGURE 4.7: An example of a focal profile for a healthy lens. The left vertical axis is where beams crossing the diameter of the lens, and the right vertical axis is where where those beams fall on the screen. All beams intersect near the same distance, indicating that the lens is able to focus light well.

Back Vertex Distance & Focal Length Variability

Back vertex distance and focal length variability are two ways to quantify the health of a lens by describing its ability to refract beams of light correctly.

Back vertex distance is a measure of focal length and represents the distance between where a beam of light enters the lens and where it crosses the optical axis. On a focal profile (Figure 4.7), the optical axis is represented by the $y = 0$ line.

The information required to describe one beam consists of two sets of coordinates (defining the beam entrance position and then where that beam falls on the screen). BVD values can be calculated by obtaining the equation of the line formed by these two points and then calculating the x-value that corresponds to a y-value of zero. This process is described mathematically as follows:

One data point consists of two sets of coordinates (x_1, y_1) and (x_2, y_2). These represent beam locations at the lens and screen, and can be named $(x_{\text{lens}}, y_{\text{lens}})$ and $(x_{\text{screen}}, y_{\text{screen}})$ for clarity, and are illustrated in Figure 4.8:

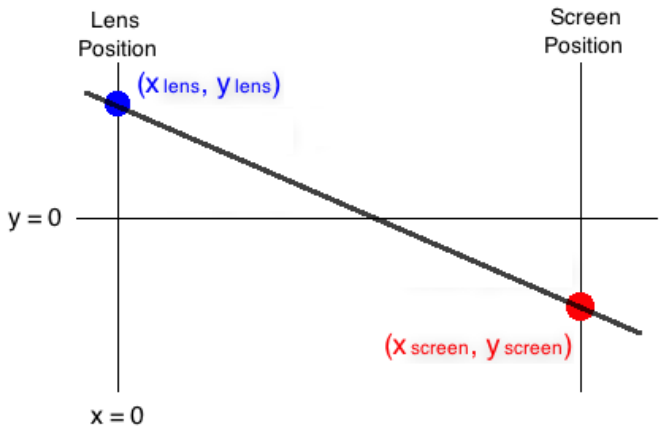

FIGURE 4.8: A diagram showing the line formed by one lens data point. The data point is made up of two coordinates: where the beam enters the lens (left), and where the beam falls on the screen (right).

$$x_{\text{lens}} = x_1 = \text{lens position}$$
$$y_{\text{lens}} = y_1 = \text{beam entrance position } \textit{(beam eccentricity)}$$
$$x_{\text{screen}} = x_2 = \text{distance from lens to screen}$$
$$y_{\text{screen}} = y_2 = \text{position of beam falling on screen } \textit{(screen eccentricity)}$$

The equation of the line formed by these two points (i.e., the path along which the beam travels from the lens to the screen) can be expressed as:

$$y = \left(\frac{y_{\text{screen}} - y_{\text{lens}}}{x_{\text{screen}} - x_{\text{lens}}} \right) x + y_{\text{lens}} \tag{4.1}$$

By assuming that the lens sits at a distance of zero (i.e., $x_{\text{lens}} = 0$), the equation can be simplified to:

$$y = \left(\frac{y_{\text{screen}} - y_{\text{lens}}}{x_{\text{screen}}} \right) x + y_{\text{lens}} \tag{4.2}$$

Back vertex distance is defined as the distance from the lens to the focal point. The focal point in this context is the distance from the lens at which the beam crosses the optical axis, which is defined as the $x = 0$ line. In other words, finding BVD is done by rearranging Equation 4.2 to solve for the x value at which $y = 0$. These steps are shown in the following equations, and conclude by giving the equation for BVD in Equation 4.9.

$$y - y_{\text{lens}} = \left(\frac{y_{\text{screen}} - y_{\text{lens}}}{x_{\text{screen}}} \right) x \tag{4.3}$$

$y = 0$, so

$$-y_{\text{lens}} = \left(\frac{y_{\text{screen}} - y_{\text{lens}}}{x_{\text{screen}}} \right) x \tag{4.4}$$

$$-\frac{y_{\text{lens}}}{x} = \frac{y_{\text{screen}} - y_{\text{lens}}}{x_{\text{screen}}} \tag{4.5}$$

$$-\frac{x}{y_{\text{lens}}} = \frac{x_{\text{screen}}}{y_{\text{screen}} - y_{\text{lens}}} \tag{4.6}$$

$$-x = \left(\frac{x_{\text{screen}}}{y_{\text{screen}} - y_{\text{lens}}} \right) (y_{\text{lens}}) \tag{4.7}$$

$$-x = \frac{(x_{\text{ screen}})(y_{\text{ lens}})}{y_{\text{ screen}} - y_{\text{ lens}}} \tag{4.8}$$

$$\text{BVD} = x = \frac{(y_{\text{ lens}})(x_{\text{ screen}})}{y_{\text{ lens}} + y_{\text{ screen}}} \tag{4.9}$$

The BVD for a single lens can be expressed as the mean of all individual beam BVDs across it. The standard error of this value is referred to as focal length variability (FLV), as shown in Equation 4.10, where SEM_{BVD} is the standard error of the mean of the set of all BVD values across the lens, σ_{BVD} is the standard deviation of the set of all BVD values across the lens, and $n_{\text{ lenses}}$ is the number of BVD values obtained for that lens.

$$\text{FLV} = \text{SEM}_{\text{BVD}} = \frac{\sigma_{\text{BVD}}}{n_{\text{ lenses}}} \tag{4.10}$$

FLV values are used to quantify the uniformity of all focal lengths across the lens diameter. In other words, a small FLV value indicates that the focal point is well-defined and that most beams pass through the same point with little deviation. A lens with a larger FLV value would have a comparatively poorly-defined focal point, and beams would have less consistency in how closely they all pass through the same point.

4.3 Lens Irradiation

Lens irradiation was performed in three experiments over a three month period (one experiment in each of January, February, and March 2019). For each experiment, either 16 or 17 rainbow trout were obtained from Linwood Acres Trout Farm. Lenses were excised immediately upon arrival to the laboratory as described in Section 4.1.2. Lenses were put into culture medium as described in Section 4.1.3 and

were left overnight, in order to acclimatize to culture conditions, with irradiations taking place the following day.

All lenses in each experiment were separated into groups of 5 to 8 lenses. The 24-well plates used to house the lenses during culturing have a built-in well labelling grid which was used for group assignments. Each group was assigned to a certain dose point, with one group per experiment being assigned to be the control. For example, the lenses in row 'A' were the 1 Gy group, row 'B' was the 2 Gy group, and row 'C' was the control group). The well-labelling system was also used to differentiate between individual lenses within a group (i.e., 'B3' always refers to the lens in the third well of row B). Lenses were always handled one at a time and returned to their respective wells.

Each lens was assessed using the laser system before irradiation. After the assessment of initial condition, the lenses in each group were irradiated individually to their assigned dose. Lenses were irradiated after being transferred to a cuvette. Irradiation occurred in four fractions, with the cuvette being turned 90° between each one. This was done to account for the depth-dose variation across the lens diameter and also for the changes in the photon energy spectrum seen by the various depths of the lens (as described in Section 3.3). Control lenses were put through the same procedure, but without X-ray exposure, in order to account for any stress caused by handling or temperature changes experienced by lenses being briefly removed from culture conditions.

Lenses were assessed using the laser system every day post irradiation, and FLV values were calculated for each lens every day that the experiment ran, starting from one day before irradiation and continuing until approximately one week after irradiation. The end-point of the experiments was determined when the lenses had deteriorated enough to make laser analysis difficult or no longer useful (e.g., if only some of the beams make it through the lens due to lens clouding, then this does not necessarily give a representative analysis of the lens as a whole). FLV values among dose groups were compared to determine whether any of the groups had statistically higher FLV values over the controls, which would indicate that the radiation had had an effect on the lenses' ability to refract light.

4.3.1 Lens Irradiation Results

After characterization experiments had been completed, lens irradiation and analysis took place. Lenses were irradiated in four fractionated doses, with the cuvette being turned 90°between each. This ensured dose uniformity throughout the lens, as opposed to irradiating in one fraction and having the front-facing surface experience a higher dose than the opposite side of the lens (even though the periphery of each lens still receives a higher dose than the core, as discussed in Section 3.3.1).

The number of lenses in each dose group as well as the period of successful culturing are summarized in Table 4.1. The labelling system adds a letter for the experiment number, allowing every lens across all three experiments to have a unique label. For example, 'JB3' refers to the third lens in row B in the first of the three experiments. Note that 'J', 'F', and 'M' are used as prefixes to differentiate lenses with the same well labels from different experiments.

TABLE 4.1: A summary of the number of lenses in each experiment, as well as the group labelling system. The first letter in the label refers to the month (January, February, or March), and the second refers to the group.

Label	Number of Lenses	Dose to Lens Core (Gy)	Dose to Lens Surface (Gy)
JD	6	Exp. 1 Control	
JB	6	0.044 ± 0.001	0.047 ± 0.002
JC	6	0.088 ± 0.001	0.094 ± 0.002
FA	7	Exp. 2 Control	
FB	7	0.186 ± 0.001	0.196 ± 0.002
FC	8	0.298 ± 0.001	0.315 ± 0.002
FD	7	0.337 ± 0.002	0.399 ± 0.002
MC	5	Exp. 3 Control	
MA	5	1.105 ± 0.002	1.170 ± 0.002
MB	5	2.210 ± 0.002	2.339 ± 0.003

TABLE 4.2: A summary of back vertex distance (BVD) and focal length variability (FLV) values for each dose group. There is no statistical difference between any group and the associated control.

Group	Dose to Lens Core (Gy)	BVD (mm)	FLV (mm)
JD	Exp. 1 Control	6.58 ± 0.12	0.09 ± 0.02
JB	0.044 ± 0.001	6.39 ± 0.09	0.07 ± 0.01
JC	0.088 ± 0.001	6.34 ± 0.07	0.07 ± 0.01
FA	Exp. 2 Control	6.45 ± 0.11	0.13 ± 0.02
FB	0.186 ± 0.001	6.45 ± 0.05	0.10 ± 0.05
FC	0.298 ± 0.001	6.42 ± 0.03	0.12 ± 0.04
FD	0.337 ± 0.002	6.56 ± 0.07	0.12 ± 0.03
MC	Exp. 3 Control	6.57 ± 0.14	0.13 ± 0.04
MA	1.105 ± 0.002	6.46 ± 0.04	0.13 ± 0.04
MB	2.210 ± 0.002	6.45 ± 0.18	0.14 ± 0.06

Each lens was analyzed using the laser focal analysis system as described in Section 4.2.2. Analysis continued until lenses were no longer suitable for evaluation (that is, until enough clouding developed to block a significant number of the laser beams used in the analysis method). This time period increased over the course of the experiments. The first and second groups of lenses were suitable for evaluation for seven days, while the third group maintained transparency for twelve days. The back vertex distance and focal length variability were calculated for each lens in each dose group, and the results are summarized in Table 4.2. FLV values are compared between dose groups in Figure 4.9.

Reviewing the BVD and FLV data in Table 4.2 and Figure 4.9 shows that none of the dose groups have BVD or FLV values that differ statistically from the corresponding control group. Though there is some statistical difference among groups from different experiments, these comparisons are invalid for a number of reasons. For instance, there is the potential that there were slight differences in experimental conditions among the three rounds of experiments that would be reflected in

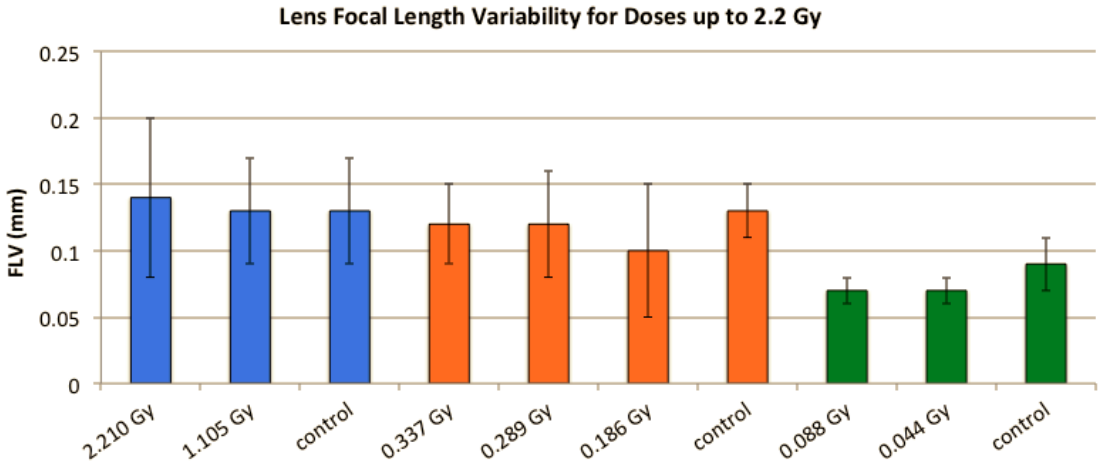

FIGURE 4.9: A summary of all focal length variability (FLV) values for all dose groups. Separate experiments are separated by colour, with a control group within each experiment.

the control group of that experiment, but not in the control group of other experiments. Additionally, slight improvements were made to the lens dissection and handling procedures between experiments, which also removes the possibility of comparing any group to another group from a separate experiment.

Overall, there are a number of differences between experiments that can be minimized, but not eliminated when performing biological experiments, and therefore the appropriate conclusion to draw from this data is that none of the lens groups had FLV values that were statistically different than the control groups.

4.3.2 Discussion of Lens Dose Response

Over the course of three experiments, groups of lenses were irradiated to 0.044 Gy, 0.088 Gy, 0.186 Gy, 0.289 Gy, 0.337 Gy, 1.105 Gy, and 2.210 Gy. Lens response was assessed by measuring back vertex distance (BVD) and focal length variability (FLV) for each lens in the experiment, including control lenses. Statistical analysis of these measurements showed that none of the dose groups was statistically different from control. This analysis was performed based on the standard error of the experimentally obtained BVD and FLV values. Therefore, there are no measurable

changes in refractive quality in the lenses during the week following irradiation up to 2 Gy.

From a physiological perspective, this could be due to the timeline of the migration of lens cells towards the lens core. The only actively dividing cells in the lens are on the surface in the epithelial layer. As these cells divide, they layer over one another and migrate towards the core of the lens. It is possible that the experiment did not monitor the lenses for long enough for any of the epithelial cells to actually migrate a significant distance into the lens. Therefore, any change in refractive quality that may have occurred to these cells as a result of radiation dose would not have been visible over the course of these experiments. It is possible that if the lenses could be successfully kept in culture for a longer time period, then refractive changes could be measurable as the epithelial cells migrated through the periphery.

One of the differences in experimental conditions that was encountered in this work was a difference in time periods of successful culturing. Over the course of the three months during which experiments took place, there were improvements made to the dissection and culturing procedures. Together with improved skill over these months, the overall timespan over which lenses were kept in good condition increased throughout the experiments. During the first two sets of experiments, lenses remained transparent enough for laser analysis for seven days. This increased to twelve days for the final set of experiments. It is possible that this timespan of good optical quality could continue to increase and produce a larger set of data in future experiments.

Another possibility is that doses of up to 2 Gy do not produce damage that is observable macroscopically in the short term because of the relatively high D_{10} dose for human lens epithelial cells (HLECs). The D_{10} value represents the dose required to reduce a population of cells to one-tenth their original value, and is a measure of the radiosensitivity of a particular cell type. HLECs have a D_{10} of 3.53 Gy, which is almost double the highest dose given to the lenses in these experiments. Additionally, a study of HLECs found that irradiating these cells with a D_{10} dose did not affect the cells' viability, but only caused a delay in the growth of the colony [45]. The study considered only the cells' ability to form

colonies (i.e., their mitotic activity), and did not assess their performance in terms of maintaining transparency in vivo or in organ culture, and therefore it is not possible to draw conclusions from this data. However, the findings do suggest that lens cells themselves are able to withstand doses much higher than the 2 Gy used in these experiments. As with the previous suggestion, it is possible that the cells, though not damaged enough to be killed by the radiation, could be damaged in a way that would affect their transparency after their migration towards the core. The same study also showed that lens cell colony growth was delayed for longer than the lenses in these experiments were kept in culture. Therefore, if there was a measurable effect in the lenses from this growth delay, then it would not be visible unless the culturing and monitoring period was longer.

Overall, there are a number of reasons why there might be no measurable change in refractive index in the lenses for the week following irradiation, and only two of those possibilities have been discussed here. Both of these hypotheses could be investigated by designing a new set of culturing conditions that could maintain the lenses in good health for a longer period of time. However, it is possible that the length of time that would be required to see the effects of these irradiations in culture may be longer than could be reasonably expected from organ culture methods.

Chapter 5

Conclusions

5.1 Overall Summary

The objective of this work is to contribute to the study of radiation effects in non-human biota and potentially to the study of eye-lens damage in humans by investigating the effects of low-energy X-rays on the lenses of rainbow trout (*Oncorhynchus mykiss*).

This work is motivated by the recent interests of the ICRP as well as the CNSC. The ICRP has updated its recommendations on eye lens dose limits and radiation effect thresholds, which has prompted the CNSC to propose lowering the annual limit for occupational dose to the human eye. This change has stimulated renewed interest in eye-lens dosimetry and research on radiation effects in the lens. The ICRP has also underlined the importance of the protection of the environment, and this prompted a discussion on possible radiation effects on the eye lens of non-human biota. Studying radiation effects in fish eye-lenses is relevant towards both these topics. The research knowledge gained from studying fish eye-lenses could also be transferable (to some degree) to understanding radiation effects in human lenses because of the anatomical and physiological similarities among the ocular systems of all vertebrates.

The use of rainbow trout lenses in these experiments is in agreement with ICRP's recommendations for moving forward in environmental radioprotection. The ICRP

has suggested the use of a trout as the reference animal for freshwater fish based on certain aspects of trout life cycles compared to other salmonids, as well as on their geographical prevalence and representation in ecosystems. Studying Reference Plants and Animals is part of ICRP's goal of working towards gaining a more comprehensive understanding of radiation effects in non-human biota [8].

A review of damage assessment methods in eye-lens research showed that a simple and useful way of measuring changes in otherwise healthy lenses is laser focal analysis. This method consists of sending a thin beam of light through a lens in such a way that the refraction of the beam can be measured. This is repeated for several beam entrance positions across the lens diameter to form a focal profile for qualitative assessment of lens health. Using the refraction data to calculate the focal lengths of individual beams can then be used to determine focal length variability (FLV) for a particular lens, or for a group of lenses. FLV values provide quantitative measures of lens health in terms of refractive capacity. Comparing FLV values for irradiated lenses and control lenses can show whether there is a significant difference in lens function between the groups. The purpose of this study was to determine whether measuring FLV could give an indication of the early effects of radiation on lens health.

An Amptek Mini-X X-ray generator was used to irradiate lenses with low-energy X-rays to several dose points up to 2 Gy. Prior to irradiation, the Mini-X was characterized, showing that at the irradiation voltage of 40 kV, the half-value thickness was 0.2 mm in PET plastic. Average X-ray energies were also measured, and these ranged from 13 keV at the front of the lens to 16 keV at the back of the lens. These differences were due to changes in the photon energy distribution spectra for the front, middle, and back of the lens, which was measured using photon energy spectrometry. The dose rate to the centre of the lens was measured to be 0.04 Gy/min. The characterization also showed that the core of the lens would receive slightly less dose than the surface and periphery. For a 1 Gy lens-core dose, the surface of the lens would receive 1.13 Gy, scaling linearly with lens-core dose.

Lenses were excised from the eyes of rainbow trout and cultured under aseptic conditions. Lenses were divided into seven groups of 5 to 8 lenses per group.

Groups were irradiated to doses of 0.044 Gy, 0.088 Gy, 0.186 Gy, 0.298 Gy, 0.344 Gy, 1.105 Gy, and 2.210 Gy, and each lens was assessed every day for up to one week post-irradiation. None of the groups showed differences in FLV compared to the control group (FLV of 0.14 mm $\pm$ 0.06 mm for the 2 Gy group compared to 0.13 mm $\pm$ 0.04 mm for the control group).

Therefore, using a laser focal analysis system to assess focal length variability following irradiation of rainbow trout eye-lenses did not show any measurable changes in refractive capacity over the short-term period of measurement. However, if the radiation mainly affects the cells in the epithelial layer of the lens, then the lack of measurable changes may be because the observation period was not long enough to allow damaged cells to migrate towards the lens core, where changes in refraction could be more evident.

5.2 Improvements on Experimental Methods

Over the course of these experiments, several instances occurred where a better experimental design became clear for future work. Many of these possible improvements pertain to the dissection and culturing procedures. Some are related to the laser focal analysis system.

During the early dissections, the method was not as refined as in later dissections. One of the ways in which lens excision was improved was the incision into the sclera. In early dissections, the sclera was cut almost the entire way around the equator, then lifted off in order to expose the lens, which was then removed. As dissection work progressed, the incisions were shortened to two or three scissor cuts, instead of the ten or so that are needed to cut around the circumference of the sclera. The lens and vitreous body could then be removed from the lens by applying gentle pressure to the side of the sclera opposite the incision. This removed a significant amount of the risk of accidentally touching a lens with the dissection instruments, and shortened the excision time considerably. This dissection technique should be employed in all future studies of this nature.

Another improvement was also implemented during later dissections. As familiarity with the dissection procedure increased, the frequency of preserving the main muscle and ligament attached to the lens also increased. In later experiments, most lenses were able to be handled using only their attached muscle or ligament, instead of needing to scoop the lens between containers using instruments, which involved direct contact with the lens.

Improvements of the procedures for future work are mainly focused on the laser analysis system. Automation of the system could be a significant improvement, since differences in lens positioning and laser beam movement could be minimized. The replacement of the grid screen used in these experiments with a video camera sensor is another change that could be simpler to implement, and would provide significant improvements in analysis. Namely, assessing beam spread and position with an image analysis software to quantify the size and uniformity of the laser beam spot size on the screen would reduce operator measurement error or bias, and could give higher-quality quantitative measurements.

5.3 Future Work

While the damage assessment method used in these experiments did not show a measurable change in lens focal capacity, there are several possible explanations, some of which have been offered in the discussion of lens dose response. Moving forward, there are some aspects of the experiment that could be expanded upon or assessed in a different way to evaluate lens damage.

The main aspect of the findings in these experiments that should be considered for future work is that dose from low-energy X-rays did not produce changes in refraction across the lenses in the short term. This is different from similar studies using ultraviolet radiation which did show measurable changes in lens refraction over the same time period used in this current work. Therefore, the differences between these radiation types could be assessed to hypothesize which differences could be responsible for the response to ultraviolet and the non-response to X-rays.

The radiosensitivity of lens epithelial cells is another factor that can be considered in future experiments, as well as cell cycle characteristics and the migration time of cells towards the lens core. The migration time could play an important role in determining when refraction changes occur, based on the premise that cells that are damaged while in the epithelial layers may not express this damage in a measurable way until they differentiate and migrate towards the lens-core.

Another potential factor to consider is the concentration of various crystallin proteins in the lens fibre cells, since these protein concentrations play an important role in determining the refraction across a lens. The crystallin concentrations could be affected by radiation either through direct interaction (i.e., crystallins that are already present in lens fiber cells in peripheral layers), or by hindering their ability to be expressed correctly during future differentiation (i.e., lens epithelial cells which have not yet begun to express crystallins). A more targeted review of the literature about the response of lens crystallin proteins to ionizing radiation could be useful in identifying processes that may be relevant to measuring lens response to radiation.

Bibliography

[1] ICRP, "International Recommendations on Radiological Protection: Revised by the International Commission on Radiological Protection at the Sixth International Congress of Radiology, London, July 1950", *Br. J. Radiol.*, vol. 24, p. 10, 1951.

[2] ICRP, "Recommendations of the International Commission on Radiological Protection. Br. J. Radiol. Suppl. 6.", *Ann. ICRP*, vol. 28, 1955. [Online]. Available: http://www.icrp.org/publication.asp?id=1954%20Recommendations.

[3] ICRP, "Statement on Tissue Reactions", 2011. [Online]. Available: www.icrp.org/docs/2011%20Seoul.pdf.

[4] ICRP, "ICRP Statement on Tissue Reactions / Early and Late Effects of Radiation in Normal Tissues and Organs – Threshold Doses for Tissue Reactions in a Radiation Protection Context. ICRP Publication 118.", *Ann. ICRP*, vol. 41, 2012.

[5] CNSC, *Discussion Paper for Public Consultation: DIS-13-01: Proposals to Amend the Radiation Protection Regulations*, Aug. 2013. [Online]. Available: http://www.nuclearsafety.gc.ca/eng/acts-and-regulations/consultation/comment/d-13-01.cfm (visited on 06/18/2019).

[6] ICRP, "1990 Recommendations of the International Commission on Radiological Protection. ICRP Publication 60.", *Ann. ICRP*, vol. 21, p. 10, 1991.

[7] ICRP, "A Framework for Assessing the Impact of Ionising Radiation on Non-human Species. ICRP Publication 91.", *Ann. ICRP*, vol. 33, 2003.

[8] ICRP, "Environmental Protection - the Concept and Use of Reference Animals and Plants. ICRP Publication 108.", *Ann. ICRP*, vol. 38, 2008. [Online]. Available: http://www.icrp.org/publication.asp?id=ICRP%20Publication%20108.

[9] T. D. Lamb, S. P. Collin, and E. N. Pugh, "Evolution of the vertebrate eye: Opsins, photoreceptors, retina and eye cup", en, *Nature Reviews Neuroscience*, vol. 8, no. 12, pp. 960–976, Dec. 2007, ISSN: 1471-003X, 1471-0048. DOI: 10.1038/nrn2283. [Online]. Available: http://www.nature.com/articles/nrn2283 (visited on 06/19/2019).

[10] R. H. Kröger, "Optical plasticity in fish lenses", en, *Progress in Retinal and Eye Research*, vol. 34, pp. 78–88, May 2013, ISSN: 13509462. DOI: 10.1016/j.preteyeres.2012.12.001. [Online]. Available: https://linkinghub.elsevier.com/retrieve/pii/S1350946212000845 (visited on 05/14/2019).

[11] O. Khorramshahi, J. M. Schartau, and R. H. Kröger, "A complex system of ligaments and a muscle keep the crystalline lens in place in the eyes of bony fishes (teleosts)", en, *Vision Research*, vol. 48, no. 13, pp. 1503–1508, Jun. 2008, ISSN: 00426989. DOI: 10.1016/j.visres.2008.03.017. [Online]. Available: https://linkinghub.elsevier.com/retrieve/pii/S0042698908001508 (visited on 05/14/2019).

[12] J. G. Sivak, "Through the Lens Clearly: Phylogeny and Development The Proctor Lecture", *Investigative ophthalmology & visual science*, vol. 45, no. 3, pp. 740–747, 2004. [Online]. Available: http://iovs.arvojournals.org/article.aspx?articleid=2181739 (visited on 04/25/2017).

[13] N. Laycock, K. Schirmer, N. Bols, and J. Sivak, "Optical Properties of Rainbow Trout Lenses after in vitro Exposure to Polycyclic Aromatic Hydrocarbons in the Presence or Absence of Ultraviolet Radiation", en, *Experimental Eye Research*, vol. 70, no. 2, pp. 205–214, Feb. 2000, ISSN: 00144835. DOI: 10.1006/exer.1999.0774. [Online]. Available: https://linkinghub.elsevier.com/retrieve/pii/S0014483599907741 (visited on 06/19/2019).

[14] A. E. Griep, "Cell cycle regulation in the developing lens", *Seminars in Cell & Developmental Biology*, vol. 17, no. 6, pp. 686–697, Dec. 2006, ISSN: 10849521. DOI: 10.1016/j.semcdb.2006.10.004. [Online]. Available: https://

linkinghub.elsevier.com/retrieve/pii/S1084952106001066 (visited on 06/19/2019).

[15] H. Šikić, Y. Shi, S. Lubura, and S. Bassnett, "A full lifespan model of vertebrate lens growth", en, *Royal Society Open Science*, vol. 4, no. 1, p. 160 695, Jan. 2017, ISSN: 2054-5703. DOI: 10.1098/rsos.160695. [Online]. Available: http://rsos.royalsocietypublishing.org/lookup/doi/10.1098/rsos.160695 (visited on 06/19/2019).

[16] S. Bassnett, "On the mechanism of organelle degradation in the vertebrate lens", *Experimental Eye Research*, vol. 88, no. 2, pp. 133–139, Feb. 2009, ISSN: 00144835. DOI: 10.1016/j.exer.2008.08.017. [Online]. Available: https://linkinghub.elsevier.com/retrieve/pii/S0014483508002984 (visited on 06/19/2019).

[17] R. I. Freshney, *Culture of animal cells: a manual of basic technique and specialized applications*, en, 6th ed. Hoboken, N.J: Wiley-Blackwell, 2010, OCLC: ocn553361168, ISBN: 978-0-470-52812-9.

[18] G. R. Merriam and A. Szechter, "The Relative Radiosensitivity of Rat Lenses as a Function of Age", *Radiation Research*, vol. 62, no. 3, p. 488, Jun. 1975, ISSN: 00337587. DOI: 10.2307/3574142. [Online]. Available: https://www.jstor.org/stable/3574142?origin=crossref (visited on 06/23/2019).

[19] F Schaeffel, H Wilhelm, and E Zrenner, "Inter-individual variability in the dynamics of natural accommodation in humans: Relation to age and refractive errors.", *The Journal of Physiology*, vol. 461, no. 1, pp. 301–320, Feb. 1993, ISSN: 00223751. DOI: 10.1113/jphysiol.1993.sp019515. [Online]. Available: http://doi.wiley.com/10.1113/jphysiol.1993.sp019515 (visited on 06/23/2019).

[20] P. E. Malkki and R. H. H. Kröger, "Visualization of chromatic correction of fish lenses by multiple focal lengths", *Journal of Optics A: Pure and Applied Optics*, vol. 7, no. 11, pp. 691–700, Nov. 2005, ISSN: 1464-4258, 1741-3567. DOI: 10.1088/1464-4258/7/11/012. [Online]. Available: http://stacks.iop.org/1464-4258/7/i=11/a=012?key=crossref.74fd784aaa58f0f7eda412dd53728551 (visited on 04/25/2017).

[21] J. M. Schartau, B. Sjögreen, Y. L. Gagnon, and R. H. Kröger, "Optical Plasticity in the Crystalline Lenses of the Cichlid Fish Aequidens pulcher", *Current Biology*, vol. 19, no. 2, pp. 122–126, Jan. 2009, ISSN: 09609822. DOI: 10.1016/j.cub.2008.11.062. [Online]. Available: https://linkinghub.elsevier.com/retrieve/pii/S0960982208016229 (visited on 06/23/2019).

[22] A. P. Cullen, C. A. Monteith-McMaster, and J. G. Sivak, "Lenticular changes in rainbow trout following chronic exposure to UV radiation", en, *Current Eye Research*, vol. 13, no. 10, pp. 731–737, Jan. 1994, ISSN: 0271-3683, 1460-2202. DOI: 10.3109/02713689409047007. [Online]. Available: http://www.tandfonline.com/doi/full/10.3109/02713689409047007 (visited on 02/26/2019).

[23] V Bantseev, K. L. Moran, D. G. Dixon, J. R. Trevithick, and J. G. Sivak, "Optical properties, mitochondria, and sutures of lenses of fishes: A comparative study of nine species", en, *Canadian Journal of Zoology*, vol. 82, no. 1, pp. 86–93, Jan. 2004, ISSN: 0008-4301, 1480-3283. DOI: 10.1139/z03-223. [Online]. Available: http://www.nrcresearchpress.com/doi/abs/10.1139/z03-223 (visited on 04/25/2017).

[24] M. C. Campbell and A. Hughes, "An analytic, gradient index schematic lens and eye for the rat which predicts aberrations for finite pupils", *Vision Research*, vol. 21, no. 7, pp. 1129–1148, 1981. DOI: 10.1016/0042-6989(81)90016-X.

[25] J. A. Weerheim and G Sivak, "Scanning laser measure of optical quality of the cultured crystalline lens", *Ophthal. Physiol. Opt.*, vol. 12, p. 9, 1992.

[26] A. Dovrat and J. G. Sivak, "Long-term Lens Organ Culture System with a Method for Monitoring Lens Optical Quality", *Photochemistry and Photobiology*, vol. 81, no. 3, p. 502, 2005, ISSN: 0031-8655. DOI: 10.1562/2004-10-20-IR-346.1. [Online]. Available: http://doi.wiley.com/10.1562/2004-10-20-IR-346.1 (visited on 04/25/2017).

[27] J. O'Brien, I. Wilson, T. Orton, and F. Pognan, "Investigation of the Alamar Blue (resazurin) fluorescent dye for the assessment of mammalian cell cytotoxicity: Resazurin as a cytotoxicity assay", *European Journal of Biochemistry*, vol. 267, no. 17, pp. 5421–5426, Sep. 2000, ISSN: 00142956. DOI:

10.1046/j.1432-1327.2000.01606.x. [Online]. Available: http://doi.wiley.com/10.1046/j.1432-1327.2000.01606.x (visited on 06/23/2019).

[28] O. M. Oriowo, A. P. Cullen, K. Schirmer, B. R. Chou, N. C. Bols, and J. G. Sivak, "Evaluation of a Porcine Lens and Fluorescence Assay Approach for In Vitro Ocular Toxicological Investigations", en, *Alternatives to Laboratory Animals*, vol. 30, no. 5, pp. 505–513, Sep. 2002, ISSN: 0261-1929, 2632-3559. DOI: 10.1177/026119290203000504. [Online]. Available: http://journals.sagepub.com/doi/10.1177/026119290203000504 (visited on 06/23/2019).

[29] H.-Y. Youn, K. L. Moran, O. M. Oriowo, N. C. Bols, and J. G. Sivak, "Surfactant and UV-B-induced damage of the cultured bovine lens", *Toxicology in Vitro*, vol. 18, no. 6, pp. 841–852, Dec. 2004, ISSN: 08872333. DOI: 10.1016/j.tiv.2004.04.007. [Online]. Available: https://linkinghub.elsevier.com/retrieve/pii/S0887233304000682 (visited on 06/23/2019).

[30] S. Iwata, "Effect of temperature on the rainbow trout lens", *Current Eye Research*, vol. 4, no. 4, pp. 441–446, Jan. 1985, ISSN: 0271-3683, 1460-2202. DOI: 10.3109/02713688509025158. [Online]. Available: http://www.tandfonline.com/doi/full/10.3109/02713688509025158 (visited on 06/23/2019).

[31] M. Hikida and S. Iwata, "In Vitro Subacute Cataractogenic Study in Rainbow Trout Lens", *J. Pharmacobio-Dyn.*, vol. 10, pp. 443–448, 1987. [Online]. Available: https://www.jstage.jst.go.jp/article/bpb1978/10/9/10_9_443/_pdf.

[32] M. Linetsky, V. G. Chemoganskiy, F. Hu, and B. J. Ortwerth, "Effect of UVA Light on the Activity of Several Aged Human Lens Enzymes", *Investigative Opthalmology & Visual Science*, vol. 44, no. 1, p. 264, Jan. 2003, ISSN: 1552-5783. DOI: 10.1167/iovs.02-0597. [Online]. Available: http://iovs.arvojournals.org/article.aspx?doi=10.1167/iovs.02-0597 (visited on 06/23/2019).

[33] N. Azzam and A. Dovrat, "Long-term lens organ culture system to determine age-related effects of UV irradiation on the eye lens", *Experimental Eye Research*, vol. 79, no. 6, pp. 903–911, Dec. 2004, ISSN: 00144835. DOI: 10.1016/j.exer.2004.06.021. [Online]. Available: https://linkinghub.elsevier.com/retrieve/pii/S0014483504001769 (visited on 06/23/2019).

[34] E. Markiewicz, S. Barnard, J. Haines, M. Coster, O. van Geel, W. Wu, S. Richards, E. Ainsbury, K. Rothkamm, S. Bouffler, and R. A. Quinlan, "Non-linear ionizing radiation-induced changes in eye lens cell proliferation, cyclin D1 expression and lens shape", en, *Open Biology*, vol. 5, no. 4, pp. 150 011–150 011, Apr. 2015, ISSN: 2046-2441. DOI: 10.1098/rsob.150011. [Online]. Available: http://rsob.royalsocietypublishing.org/cgi/doi/10.1098/rsob.150011 (visited on 04/25/2017).

[35] K. Rothkamm, I. Kruger, L. H. Thompson, and M. Lobrich, "Pathways of DNA Double-Strand Break Repair during the Mammalian Cell Cycle", *Molecular and Cellular Biology*, vol. 23, no. 16, pp. 5706–5715, Aug. 2003, ISSN: 0270-7306. DOI: 10.1128/MCB.23.16.5706-5715.2003. [Online]. Available: http://mcb.asm.org/cgi/doi/10.1128/MCB.23.16.5706-5715.2003 (visited on 06/23/2019).

[36] A. Dovrat, R. Berenson, E. Bormusov, A. Lahav, T. Lustman, N. Sharon, and L. Schächter, "Localized effects of microwave radiation on the intact eye lens in culture conditions", en, *Bioelectromagnetics*, vol. 26, no. 5, pp. 398–405, Jul. 2005, ISSN: 0197-8462, 1521-186X. DOI: 10.1002/bem.20114. [Online]. Available: http://doi.wiley.com/10.1002/bem.20114 (visited on 04/25/2017).

[37] ICRP, "The 2007 Recommendations of the International Commission on Radiological Protection. ICRP Publication 103. Ann. ICRP 37 (2-4).", *Ann. ICRP*, 2007. [Online]. Available: http://www.icrp.org/publication.asp?id=ICRP%20Publication%20103.

[38] N. Hamada, "Ionizing radiation sensitivity of the ocular lens and its dose rate dependence", *International Journal of Radiation Biology*, vol. 93, no. 10, pp. 1024–1034, Oct. 2017, ISSN: 0955-3002, 1362-3095. DOI: 10.1080/09553002.2016.1266407. [Online]. Available: https://www.tandfonline.com/doi/full/10.1080/09553002.2016.1266407 (visited on 06/24/2019).

[39] Y. Belkacémi, P. Rat, G. Piel, M.-O. Christen, E. Touboul, and J.-M. Warnet, "Lens Epithelial Cell Protection by Aminothiol WR-1065 and Anetholedithiolethione from Ionizing Radiation", *Int. J. Cancer (Radiati. Oncol. Invest.)*, vol. 96 (Suppl.) Pp. 15–26, 2001. (visited on 06/14/2019).

[40] T. V. Azizova, E. V. Bragin, N. Hamada, and M. V. Bannikova, "Risk of Cataract Incidence in a Cohort of Mayak PA Workers following Chronic Occupational Radiation Exposure", en, *PLOS ONE*, vol. 11, no. 10, G. E. Woloschak, Ed., e0164357, Oct. 2016, ISSN: 1932-6203. DOI: 10.1371/journal.pone.0164357. [Online]. Available: http://dx.plos.org/10.1371/journal.pone.0164357 (visited on 06/22/2019).

[41] T. Malmstrom, "Pupil shapes and lens optics in the eyes of terrestrial vertebrates", en, *Journal of Experimental Biology*, vol. 209, no. 1, pp. 18–25, Jan. 2006, ISSN: 0022-0949, 1477-9145. DOI: 10.1242/jeb.01959. [Online]. Available: http://jeb.biologists.org/cgi/doi/10.1242/jeb.01959 (visited on 06/22/2019).

[42] E. A. Ainsbury, S. D. Bouffler, W. Dörr, J. Graw, C. R. Muirhead, A. A. Edwards, and J. Cooper, "Radiation Cataractogenesis: A Review of Recent Studies", en, *Radiation Research*, vol. 172, no. 1, pp. 1–9, Jul. 2009, ISSN: 0033-7587, 1938-5404. DOI: 10.1667/RR1688.1. [Online]. Available: http://www.bioone.org/doi/10.1667/RR1688.1 (visited on 06/22/2019).

[43] D. D. Stuart, A. P. Cullen, J. G. Sivak, and M. J. Doughty, "Optical effects of UV-A and UV-B radiation on the cultured bovine lens", *Current eye research*, vol. 13, no. 5, pp. 371–376, 1994. [Online]. Available: http://www.tandfonline.com/doi/abs/10.3109/02713689409167301 (visited on 04/25/2017).

[44] D. D. Stuart, J. G. Sivak, A. P. Cullen, J. A. Weerheim, and C. A. Monteith, "UV-B radiation and the optical properties of cultured bovine lenses", *Current Eye Research*, vol. 10, no. 2, pp. 177–184, Jan. 1991, ISSN: 0271-3683, 1460-2202. DOI: 10.3109/02713689109001746. [Online]. Available: http://www.tandfonline.com/doi/full/10.3109/02713689109001746 (visited on 06/24/2019).

[45] N. Hamada, "Ionizing radiation response of primary normal human lens epithelial cells", *PLOS ONE*, vol. 12, no. 7, G. E. Woloschak, Ed., e0181530, Jul. 2017, ISSN: 1932-6203. DOI: 10.1371/journal.pone.0181530. [Online]. Available: https://dx.plos.org/10.1371/journal.pone.0181530 (visited on 06/24/2019).

[46] U. Andley and J. Weber, "Ultraviolet action spectra for photobiological effects in cultured human lens epithelial cells", *Photochemistry and Photobiology*, vol. 62, no. 5, pp. 840–846, 1995.

[47] H.-Y. Youn, D. J. McCanna, J. G. Sivak, and L. W. Jones, "In vitro ultraviolet–induced damage in human corneal, lens, and retinal pigment epithelial cells", 2011. [Online]. Available: http://www.molvis.org/molvis/v17/a29/ (visited on 04/25/2017).

[48] K. Bannik, U. Rössler, T. Faus-Kessler, M. Gomolka, S. Hornhardt, C. Dalke, O. Klymenko, M. Rosemann, K.-R. Trott, M. Atkinson, U. Kulka, and J. Graw, "Are mouse lens epithelial cells more sensitive to gamma-irradiation than lymphocytes?", *Radiation and Environmental Biophysics*, vol. 52, no. 2, pp. 279–286, May 2013, ISSN: 0301-634X, 1432-2099. DOI: 10.1007/s00411-012-0451-8. [Online]. Available: http://link.springer.com/10.1007/s00411-012-0451-8 (visited on 06/24/2019).

[49] Y. Fujimichi and N. Hamada, "Ionizing Irradiation Not Only Inactivates Clonogenic Potential in Primary Normal Human Diploid Lens Epithelial Cells but Also Stimulates Cell Proliferation in a Subset of This Population", *PLoS ONE*, vol. 9, no. 5, M. Duncan, Ed., e98154, May 2014, ISSN: 1932-6203. DOI: 10.1371/journal.pone.0098154. [Online]. Available: https://dx.plos.org/10.1371/journal.pone.0098154 (visited on 06/19/2019).

[50] J. M. Davis, Ed., *Animal Cell Culture: Essential Methods*, en. Hertfordshire, UK: Wiley-Blackwell, 2011.

[51] A. P. Fraise, J.-Y. Maillard, and S. Sattar, Eds., *Principles and practice of disinfection, preservation, and sterilization*, en, 5th ed. Chichester, West Sussex: John Wiley & Sons, 2012, ISBN: 978-1-4443-3325-1.

[52] "Miniature X-Ray Source", Ametek, Bedford, MA, Specifications Sheet. [Online]. Available: www.amptek.com/pdf/minix.pdf (visited on 06/04/2019).

[53] "Exradin Detectors", Standard Imaging, Product Information Exradin BR 1180-27. [Online]. Available: https://www.standardimaging.com/uploads/manuals/Exradin_BR_1180-27.pdf (visited on 06/07/2019).

[54] J. Hubbell and H. Seltzer, *X-Ray Mass Attenuation Coefficients*. [Online]. Available: https://www.nist.gov/pml/x-ray-mass-attenuation-coefficients (visited on 06/08/2019).

[55] M. Aschner, C. Suñol, and A. Bal-Price, Eds., *Cell culture techniques*, en, ser. Springer protocols 56. New York, N.Y: Humana Press, 2011, OCLC: ocn703374713, ISBN: 978-1-61779-076-8.